

STRESS MODULATION OF  
THE DEGREE OF SPIN POLARIZATION  
ON BULK SEMICONDUCTORS

THESIS BY  
JUAN CUAUHTÉMOC SALAZAR GONZÁLEZ

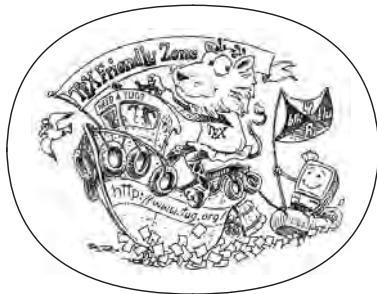


**CENTRO DE INVESTIGACIONES  
EN OPTICA, A.C.**

Department of Photonics

Master in Sciences (Optics)

February 13, 2009  
(Defended on December 11, 2008)



Juan Cuauhtémoc Salazar González: *Stress Modulation of the Degree of Spin Polarization on Bulk Semiconductors*, Master in Sciences (Optics), © December 11, 2008

**SUPERVISOR:**

Dr. Bernardo Mendoza Santoyo

**COMMITTEE:**

Dr. Raúl Alfonso Vázquez Nava

Dr. Norberto Arzate Plata

**LOCATION:**

Léon, MÉXICO

**TIME FRAME:**

December 11, 2008

Dedicated to all the people that have decided  
to be with me along this years at [CIO](#).

To those who have done that in the distance,  
like my parents Rosario Gonzalez and Juan Salazar,  
my brothers Xóchitl, Francisco and Xicoténcatl,  
and my aunt and uncle Teresa and Raúl Gonzalez.

Specially to my girlfriend Saray who has had  
the confidence to share with me her family,  
and the patience to have a long-distance relationship.



## ABSTRACT

---

The thesis work presented here is part of the research I performed under the supervision of Dr. Bernardo Mendoza during my Master in Science studies at Centro de Investigaciones en Óptica, A.C. (León, México). Its main objectives are (1) to investigate the well known fact that the optical electron spin-injection on bulk semiconductors is affected by the application of strain, and (2) to explore the possibility of modulate such phenomenon by either compressive or expansive strains.

To address this project, a simple and effective method to compute the spin injection as a function of strain (actually, of a related quantity) is proposed, considering both compressive and expansive strains.

For this purpose, the approach of density functional theory (DFT) was taken, employing pseudopotential band structures based on the local density approximation (LDA). The computational tools employed were a computer cluster and almost solely *free software* programs. At the end it is shown that the application of stress can effectively modulate, and even enhance, the optical spin-injection on bulk semiconductors.

## RESUMEN

---

El trabajo de tesis aquí presentado forma parte de las labores de investigación que realicé bajo la supervisión del Dr. Bernardo Mendoza, durante mis estudios de Maestría en Ciencias en el Centro de Investigaciones en Óptica, A.C. (León, México). Sus objetivos principales son (1) investigar el hecho conocido de que la inyección de espín electrónico es afectada por la aplicación de esfuerzos, así como (2) explorar la posibilidad de modular este fenómeno ya sea mediante esfuerzos de compresión o expansión.

Para abordar este proyecto, se implementó un método sencillo y efectivo de calcular la inyección de espín como función del esfuerzo aplicado (en realidad, de una cantidad relacionada con él), tanto en compresión como expansión.

Para este propósito se empleó el formalismo de la Teoría Funcional de la Densidad (DFT) y estructuras de bandas pseudo-potenciales basadas en la aproximación local de la densidad (LDA). Las herramientas computacionales empleadas fueron un *cluster* de cómputo y en forma casi exclusiva programas de *software libre*. Al final se muestra cómo la aplicación de un esfuerzo puede efectivamente modular, e incluso mejorar, la inyección óptica de espín en semiconductores de bulto.



## PUBLICATIONS

---

This thesis is strongly based on the ideas and techniques appeared previously in the following publications:

REFERENCE [1]. F. Nastos, J. Rioux, M. Strimas-Mackey, Bernardo S. Mendoza, and J. E. Sipe. Full band structure LDA and  $\mathbf{k} \cdot \mathbf{p}$  calculations of optical spin-injection. *Phys.Rev. B*, 76, 2007.

REFERENCE [2]. B.S. Mendoza, F. Nastos, N. Arzate and J.E. Sipe. *Phys.Rev. B*, 74, 075318 - 2006.

Indeed, the work presented here can be thought as an extension of Reference [1].





*Modern man is a mass-man; highly socialized, but very lonely.  
He is alienated from others, and confronted with a dilemma:  
afraid of close contact with another, and equally afraid to be alone.  
It is the function of trivial conversation to answer the question:  
How do I remain alone without being lonely?.*

— Erich Fromm [3]  
The Art of Being.

## ACKNOWLEDGMENTS

---

I want to acknowledge all the people that have sacrificed themselves for me. This Master's thesis is not the work of two years, is something that started a long time ago in my parents', aunts', and uncles' laps.

Special thanks to my advisor, Dr. Bernardo Mendoza Santoyo, for all his support since that undergraduate summer internship at [CIO](#) in 2002, and for all his advices on topics that sometimes have gone beyond the academic arena. He is for me an example of hard work, astuteness, and insight.

I want to express my frank gratitude to two of the closest friendships I have won during this time: my classmate Araceli Guerrero, for her sincere friendship and invaluable support, and to the group's senior doctoral student, José Luis Cabellos, who has shared with me not only his eagerness to make a script work, but also his candid friendship and funny company. For their valuable suggestions, to Dr. Norberto Arzate Plata and Dr. Raul Vázquez Nava, who revised this thesis. In general to all the members of the Surface Optics Group at [CIO](#), and all the rest of my classmates, Diana, Yenysey, Guillermo, and the singular Jorge. To Dr. Norberto Arzate, Dr. Rafael Espinosa Luna and Maximiliano for their support for my dwelling. All of you have contributed to increase what I have accomplished here at León.

Special thanks to *Departamento de Formación Académica* for all the support they gave me; particularly for the opportunity to attend (1) specialized courses like [ABINIT-2008](#), the Third Mexican Summer School on Quantum Computation and Quantum Information (thanks Dr. Venegas-Andraca for your support and thanks Dr. Macro Lanzagorta for your candid advices), (2) the summer stay at University of Toronto (thanks Prof. John Sipe!) and (3) several congresses. Special acknowledgments to Lic. Guillermina Muñoz for her complete commitment to the students' success and the kind treatment she always gave me.

In general, to the Mexican Government that, by means of the [SEP](#), has given me the opportunity to study at almost no cost since my childhood. To [CONACYT](#) for the postgraduate scholarship 204367, and to [CONCYTEG](#) for the thesis scholarship 08-04-k119-133-Anexo-2.

Last but not least, *graciñas Cris pola túa axuda co Inglés. . . e en español!*



*El hombre moderno es un hombre de las masas;  
sumamente socializado, pero muy solitario.  
Está alienado por otros, y confrontado con un dilema:  
temeroso de tener contacto cercano con otro,  
e igualmente temeroso de estar solo.  
La función de la conversación trivial [banal]  
es entonces la encargada de responder a esta pregunta:  
¿Cómo me mantengo a solas sin ser un solitario?*

— Erich Fromm [3]  
The Art of Being.

## AGRADECIMIENTOS

---

Deseo agradecer a todas aquellas personas que se han sacrificado por mí. Esta tesis de maestría no representa el trabajo de sólo dos años, sino que es algo que comenzó mucho tiempo atrás en el regazo de mis padres y de mis tíos.

Deseo agradecer en forma muy especial a mi asesor, el Dr. Bernardo Mendoza Santoyo, por todo el apoyo que me ha brindado. Tanto por aquella estancia de verano de licenciatura en el año 2002, así como por todos sus consejos que en varias ocasiones fueron mas allá del ámbito académico. Él es para mí ejemplo de trabajo arduo, astucia y visión.

Quiero expresar mi franca gratitud a dos de las más cercanas amistades que gané durante este tiempo: a mi compañera de clase, Araceli Guerrero, por su sincera amistad e invaluable apoyo, así como al estudiante doctoral José Luis Cabellos, quien no sólo ha compartido conmigo su avidez para hacer funcionar los programas, sino también su sincera y graciosa compañía. Por sus invaluable sugerencias, a los revisores de esta tesis, Dr. Norberto Arzate Plata y Dr. Raul Vázquez Nava. En general, a todos los miembros del Grupo de Superficies Ópticas del CIO, y al resto de mis compañeros de clase: Diana, Yenysey, Guillermo y al singular Jorge. Al Dr. Norberto Arzate, al Dr. Rafael Espinosa Luna y a Maximiliano por las facilidades otorgadas para mi hospedaje. Todos ustedes han contribuido a incrementar lo que he adquirido aquí en León.

De manera muy especial, a todo el Departamento de Formación Académica por el apoyo otorgado; muy en particular por la ayuda para asistir (1) a cursos y estancias de especialización, como [ABINIT-2008](#), la Segunda Escuela Mexicana en Computación Cuántica e Información Cuántica (gracias Dr. Venegas-Andraca por su apoyo logístico; gracias Dr. Macro Lanzagorta por sus consejos), (2) a la estancia de verano

en la Universidad de Toronto (¡gracias Prof. John Sipe!), y (3) a diversos congresos de la especialidad. Agradecimientos especiales a la Lic. Guillermina Muñoz por su completa entrega al éxito y desempeño de todos los estudiantes del CIO, y particularmente por el amable trato que siempre me ha brindado.

En general, al Gobierno Mexicano que, por medio de la SEP, me ha dado la oportunidad de estudiar prácticamente sin costo alguno desde mi niñez. Al CONACYT por la beca de maestría 204367, y al CONCYTEG por la beca-tesis 08-04-k119-133-Anexo-2.

Por último, pero no por ello menos importante: ¡gracias Cristina por tu ayuda con la redacción en Inglés... y Español!

## SUMMARY OF CONTENTS

---

|   |           |
|---|-----------|
| Record of Thesis Defence                          | iii       |
| Degree's Transcript                               | v         |
| List of Figures                                   | xxi       |
| List of Tables                                    | xxi       |
| <b>I BACKGROUND</b>                               | <b>1</b>  |
| 1 INTRODUCTION                                    | 3         |
| 2 ELECTRONIC SPIN                                 | 15        |
| <b>II THEORY</b>                                  | <b>21</b> |
| 3 DSP: THE DEGREE OF SPIN POLARIZATION            | 23        |
| 4 STRESS MODULATION OF DSP ON BULK SEMICONDUCTORS | 37        |
| <b>III RESULTS AND CONCLUSIONS</b>                | <b>47</b> |
| 5 EXAMPLES OF DSP MODULATION                      | 49        |
| 6 SUMMARY AND CONCLUSIONS                         | 59        |
| <b>IV APPENDIX</b>                                | <b>61</b> |
| A COMPUTATIONAL TOOLS                             | 63        |
| B POSTER PRESENTATION                             | 71        |
| BIBLIOGRAPHY                                      | 73        |
| CONCEPT INDEX                                     | 76        |



## DETAILED CONTENTS

---

Record of Thesis Defence   iii

Degree's Transcript       v

List of Figures       xxi

List of Tables       xxi

### I BACKGROUND   1

- 1 INTRODUCTION   3
  - 1.1 Motivation and Overview   3
  - 1.2 Spin Polarization   5
  - 1.3 Spin Measurement   7
  - 1.4 Spin Relaxation   8
  - 1.5 Spintronic Devices   9
  - 1.6 Objectives and Overview of this Thesis   12
- 2 ELECTRONIC SPIN   15
  - 2.1 Basic Demonstration of Spin Existence   15
  - 2.2 Spin Inclusion into the Quantum Theory   16
  - 2.3 Pauli's Description of Spin   17
  - 2.4 Pauli's Postulates   18

### II THEORY   21

- 3 DSP: THE DEGREE OF SPIN POLARIZATION   23
  - 3.1 Introduction   23
  - 3.2 Density-Matrix Equation of Motion   23
  - 3.3 Multi-scale Solution of the Equation of Motion   25
  - 3.4 Degree of Spin Polarization   31
  - 3.5 Degree of Spin Polarization   34
- 4 STRESS MODULATION OF DSP ON BULK SEMICONDUCTORS   37
  - 4.1 Objectives   37
  - 4.2 Computational Approach   37
  - 4.3 Convergence Analysis   41
  - 4.4 Stress-Induced Volumetric Change   42

### III RESULTS AND CONCLUSIONS   47

- 5 EXAMPLES OF DSP MODULATION   49
  - 5.1 Objectives   49
  - 5.2 Example 1. Bulk Silicon Study   49
  - 5.3 Example 2. Bulk Gallium Arsenide Study   54
- 6 SUMMARY AND CONCLUSIONS   59
  - 6.1 Summary   59
  - 6.2 Conclusions   60

|     |  |    |
|-----|--|----|
| IV  | APPENDIX                                     | 61 |
| A   | COMPUTATIONAL TOOLS                          | 63 |
| A.1 | “Free Software, Free Society”                | 63 |
| A.2 | Tiniba: A set of BASH Scripts                | 64 |
| A.3 | Medusa: The Computing Cluster                | 67 |
| A.4 | Performance of the Copy and Abinis Processes | 69 |
| B   | POSTER PRESENTATION                          | 71 |
|     | BIBLIOGRAPHY                                 | 73 |
|     | CONCEPT INDEX                                | 76 |



## LIST OF FIGURES

---

|           |  |    |
|-----------|--|----|
| Figure 1  | Coherent excitations                       | 24 |
| Figure 2  | Allowed and forbidden coherence terms      | 27 |
| Figure 3  | The first Brillouin zone                   | 40 |
| Figure 4  | Coherent excitations                       | 43 |
| Figure 5  | Prof. Turneure’s e-mail                    | 44 |
| Figure 6  | Convergence on k–points for bulk silicon   | 50 |
| Figure 7  | Convergence on energy cutoff on silicon    | 51 |
| Figure 8  | Convergence on conduction bands on silicon | 52 |
| Figure 9  | Stress modulation of the DSP on silicon    | 53 |
| Figure 10 | Convergence on k–points on GaAs            | 55 |
| Figure 11 | Convergence on energy cutoff on GaAs       | 56 |
| Figure 12 | Convergence on conduction bands on GaAs    | 56 |
| Figure 13 | Experimental DSP on GaAs                   | 57 |
| Figure 14 | Stress modulation of DSP on GaAs           | 57 |
| Figure 15 | Small scale DSP results                    | 60 |
| Figure 16 | TINIBA shells                              | 65 |
| Figure 17 | Medusa’s Quad processors                   | 67 |
| Figure 18 | Medusa: The cluster computer               | 68 |
| Figure 19 | Copy performance                           | 70 |
| Figure 20 | Poster at the National Congress            | 71 |

## LIST OF TABLES

---

|         |                                      |    |
|---------|--------------------------------------|----|
| Table 1 | Single- and Multi- Copy Benchmarking | 70 |
|---------|--------------------------------------|----|

## LIST OF ACRONYMS

---

Future appearance of the following acronyms are hyperlinked to this page.

|          |  |
|----------|--|
| ABINIT   | Software to compute <i>ab-initio</i> ('from first principles') properties of atoms, nuclei, and solids.                                  |
| BASH     | Bourne-Again SHell. Bash is the shell in the GNU operating system. A shell is a command language interpreter.                            |
| BZ       | Brillouin Zone   |
| CIO      | Centro de Investigaciones en Óptica, A.C.  |
| CONACYT  | Consejo Nacional de Ciencia y Tecnología   |
| CONCYTEG | Consejo de Ciencia y Tecnología del Estado de Guanajuato   |
| DARPA    | U.S. Defense Advanced Research Projects Agency   |
| DFT      | Density Functional Theory  |
| DSP      | Degree of Spin Polarization  |
| EDSR     | Electric Dipole Induced Spin Resonance   |
| GNU      | Gnu is Not Unix [Recursive acronym]  |
| GMR      | Giant Magneto Resistance Device  |
| JDOS     | Joint Density Of States  |
| LATM     | Linearized Analytic Tetrahedron Method   |
| LDA      | Local Density Approximation  |
| NMR      | Nuclear Magnetic Resonance   |
| RF       | Radio Frequency  |
| SCF      | Self-Consistent Field [method]   |
| SEP      | Secretaría de Educación Pública  |
| SPINS    | Spins IN Semiconductors  |
| TINIBA   | ABINIT written backwards. A set of bash shells to compute optical properties of materials. See <a href="#">Section A.2</a> and Ref. [4]. |

## LIST OF MNEMONICS

---

Future appearance of the following programming mnemonics are hyperlinked to this page. They refer to variables or parameters in the computer programs, either [ABINIT](#) or [TINIBA](#). They are used from [Section 4.3](#) onward (page [41](#)).

|                    |  |
|--------------------|--|
| <code>acell</code> | scAle CELL                                 |
| <code>cband</code> | Conduction BANDs                           |
| <code>ecut</code>  | Energy CUToff                              |
| <code>nband</code> | Number of BANDs (valence plus conduction). |
| <code>nkpt</code>  | Number of k-PoinTs                         |
| <code>rprim</code> | Real PRIMitive vectors                     |



Part I

BACKGROUND



INTRODUCTION

---

*Elegir es anunciar y renunciar.*

*(To choose is to announce and to renounce)*

— Enrique Rojas  
Spanish Humanist

## 1.1 MOTIVATION AND OVERVIEW

One of the most important tendencies of technology is miniaturization, to the point that in the late part of last century the term *nanotechnology* was coined to refer to devices around or below 100 nm in size. As this miniaturization continues, technologists and scientists are faced with new opportunities and awkward challenges. Essentially the tinier they become, the more scientists are faced with quantum phenomena, like quantum tunneling, spin effects, and entangled states, to mention some of the most popular. Such issues represent current areas of research for the design, control, and operation of devices at such dimensions.

Most of the technology in use over the past century was strongly based on the study, design, and use of devices based on the conduction of electricity in a vacuum, a gas, or a semiconductor medium. Such devices are called *electronic* and the conduction of such electricity constitutes an electric current <sup>1</sup>, that is, a flow of charge carriers, which may be electrons, holes, or ions. At present, another dominant device-technology arises from the integration of electronics with an ancient and older technology, namely with optics; it is called *optoelectronics*.

As mentioned above, quantum phenomena that may have interesting applications to technology are *spin effects*. Spin is an intrinsic property of elementary particles and nuclei and represents another degree of freedom for them. Bohr's theory of the atom predicts that lines in the spectra of alkali metals<sup>2</sup> should be single, but in fact, they consist of doublets. Pauli suggested that each electron could exist in two states

---

<sup>1</sup> In the International System of Units ([www.bipm.org/en/si/](http://www.bipm.org/en/si/)) the electric current is measured in Amperes, abbreviated as 'A'; one Ampere is equivalent to the flow of  $10^{18}$  electrons per second.

<sup>2</sup> Alkali metals are chemical elements in group I of the periodic table (except hydrogen): lithium, sodium, potassium, rubidium, caesium, and francium. These elements all have one electron in their outermost shell, so the energetically preferred state of achieving a filled electron shell is to lose one electron to form a singly charged positive ion, i.e. a cation. Alkali metals have the lowest ionization potentials in their respective periods, as removing the single electron from the outermost shell gives them the stable inert gas

with the same orbital motion. Uhlenbeck and Goudsmit interpreted these states as due to the spin of the electron about an axis; thus the electron is assumed to have an intrinsic angular momentum in addition to any angular momentum due to its orbital motion. Moreover, in the presence of an external magnetic field the angular momentum vector of the electron precesses<sup>3</sup> around the field direction. In such precession not all orientations of the vector to the field direction are allowed: there is a quantization so the component of the angular momentum along the direction is restricted to certain values. This phenomenon is called *space quantization*.

As seen, this quantity was originally coined in relation to *rotation of particles* around their own axis, although the concept '*rotation of a particle*' does not make sense, the quantum spin follows the same mathematical structure of quantized angular momenta, but with some peculiarities, such as non-integer quantum units of spin.

Quantum spin properties play a fundamental role in the basic theory of physics, for instance,

- Spin is a fundamental constituent of the Pauli's Principle of Exclusion, being the spin one of the four quantum numbers.
- Ultra high sensitive spectroscopic tools are based on spin effects to study spin-orbit and hyperfine interactions, pairing symmetries of high temperature superconductors and parity violation of high energy physics.
- Imaging techniques based on the manipulation of nuclear spins have played a crucial role in chemical spectroscopy and medical imaging. For instance, Nuclear Magnetic Resonance (NMR) techniques use radio frequency (RF) signals to control spins.

#### *Initial research in spin-physics*

Perhaps the first reported experiment on spin-physics is that of Wood and Ellett, where in 1923 they investigated the variations in the polarization of the fluorescence of mercury vapor excited by polarized light. With their work they discovered the depolarization of luminiscence by transverse magnetic fields, know as the Hanle effect. About 25 years later, in the 1950s, Brossel and Kastler carried out intensive research in optical polarization and electric control of atomic angular moments. Almost in the 1970s, Lampel executed experiments on the optical spin orientation of electrons in semiconductors.

configuration. Their second ionization potentials are very high, as removing an electron from a species having a noble gas configuration is very difficult.

<sup>3</sup> Precession: If a body is spinning about an axis  $OC$ , where  $O$  is a fixed point and  $C$  is rotating round an axis  $OZ$  fixed outside the body, the body is said to be precessing around  $OZ$ , which is called the precession axis [5].



*From spin-physics to spin-technology*

Devices that exploit the spin degree of freedom of electrons, holes, and nuclei are called *spintronics* and were first massively investigated around 1996 by the U.S. Defense Advanced Research Projects Agency (DARPA) in an initiative called *Magnetic Materials and Sensors*, aimed to develop such devices through spin transport electronics. This initiative was soon extended to include a broader kind of spin-based devices and was then called *Spins IN Semiconductors (SPINS)*. The term *spintronics* was then coined by S.A. Wolf et al. (see Ref. [6]), one of the principal researchers of the initiative.

According to Das Sarma on Ref. [7], spintronic devices have some important key advantages compared with conventional electronic devices, notably

**NATURAL BINARY LOGIC.** As electrons can have spin  $+1/2$  or  $-1/2$ , they led naturally to a binary logic of ones and zeroes. These values correspond to parallel and anti-parallel alignment with respect to an applied magnetic field.

**EASY MANIPULATION.** Experiments have shown that spin systems are easily manipulated by external applied magnetic or optical fields (see Najmaie et al. on Ref. [8] and Bhat et al. on Ref. [9]).

**LONG COHERENCE.** Coherence or relaxation time refers to the time spin direction tends to remain after external control is removed and spins start to decay to random directions, mainly due to spin-orbit coupling and momentum scattering; this is called *spin relaxation*. Spin coherence has been showed to be longer than those of electric charges, because electric coherence tends to be destroyed by scattering and collisional effects with defects, impurities, and other charges (see Section 1.4).

## 1.2 SPIN POLARIZATION

Ferromagnets are solid materials that, due to their large positive susceptibility, are magnetizable by weak magnetic fields. Typical ferromagnetic materials are iron, cobalt, nickel, and alloys containing them as well. Depending on the material, ferromagnets can retain their magnetization even after the magnetic field is removed<sup>4</sup>.

The permanent spin polarization in ferromagnets is called *equilibrium carrier spin polarization*, nevertheless, according to Igor Žutić et al.

*Equilibrium spin polarization*

<sup>4</sup> Ferromagnetic magnetization is due to *the growth* of ferromagnetic domains, which are regions of crystalline matter with volumes ranging from  $10^{-12}$  to  $10^{-8}\text{m}^3$ ; such domains contain atoms whose magnetic moments are aligned in the *same* direction; therefore ferromagnetic domains possess magnetic axis and moment. In an unmagnetized ferromagnet the domains are polarized at random, but if a weak magnetic field is applied,

on Ref. [10], it is not enough for spintronic applications, which rely on current flow and/or coherent manipulation of *non-equilibrium* spin polarization. The latter is created with the aid of a spin pumping source. Usually, the spin injection rate is controlled by optical, electrical, or resonant techniques. The basic principles of operation are:

**OPTICAL SPIN-ORIENTATION.** Apart from electrons, nuclei, and ions, photons also possess intrinsic angular momentum, i.e. spin, which is quantized to two values,  $S = \pm\hbar$ , corresponding to a spin direction parallel or anti-parallel to their momentum vector. Because a linear photon has an equal probability of exhibiting parallel or anti-parallel spin-orientation, it can be thought as composed of a right-circularly and a left-circularly photon, both with 1/2 probability.<sup>5</sup> When a photon is absorbed it transfers its linear momentum to the medium and if the photon is circular-polarized, it transfers angular momentum, exerting a torque on the medium.

Optical orientation of spins refers to the spin-polarization by the absorption of circular polarized light, for instance, by transference of angular momenta from circular-polarized photons to electrons. The work presented in this thesis lies in this type of spin polarization.

**ELECTRICAL SPIN-ORIENTATION.** Magnetism is the result of the motion of electrons when the circulatory current created by the angular momentum of an electron moving in its orbit produces a magnetic moment known as Bohr Magneton,<sup>6</sup>  $\mu_{\text{Bohr}} = \hbar e/2m_e$ , where  $e$  is the elementary charge,  $\hbar$  is the reduced Planck constant, and  $m_e$  is the electron rest mass.

Electrical spin-orientation refers to the spin-polarization of a sample by the transport (injection) of spin-oriented electrons. Such electrons from a magnetic electrode bonded to the sample; the transport is induced by the application of an electric current.

**RESONANT SPIN-ORIENTATION.** Nuclear spin is the vector sum of its constituent particle spins, protons and neutrons. Therefore, nuclei also possess a magnetic moment, which in the presence of an external magnetic field, precesses about the applied field direction.

---

the domains whose axis point along or close to the direction of the applied field grow at the expense of their neighbors. In a limiting case, the domain growth tends to the size of the specimen.

<sup>5</sup> A beam of light is said to be circularly polarized if its electric vector undergoes uniform rotation in the  $xy$  plane, being  $z$  the direction of propagation. Circularly polarized photons are considered right- of left-handed depending if they have positive or negative angular momentum along the direction of propagation. The convention for the correspondence between right/left and positive/negative varies in the literature (see [Yariv and Yeh](#) on Ref. [11], p. 21).

<sup>6</sup>  $\mu_{\text{Bohr}} \approx 5.8 \times 10^{-5} \text{ eV/T} \approx 927.4 \times 10^{-26} \text{ J/T}$ .

The orientation of the nuclear magnetic moment is discretized and each of these directions corresponds to different nuclear energies, whose difference depends on the applied field. The nucleus can make transitions from one state to another with the emission or absorption of electromagnetic radiation according to a selection rule. Actually, NMR is based on the adsorption of RF radiation (1 – 100 MHz): a strong variable magnetic field about 2 Teslas is applied to the sample, and then a RF field is applied at right angles and a coil detector is wound around the sample. As the strong magnetic field is varied, the spacing of the energies varies, and at certain value of the magnetic field, this spacing is such that RF radiation is strongly absorbed; this resonance produces a signal in the detector coil. The nuclear magnetic moments can be determined from the resonance spectrum, plotting the coil signal versus the applied magnetic field.

A spin-orientation technique called Electric Dipole Induced Spin Resonance (EDSR) exists, where electric RF fields give rise to internal fields coupling to the spin. Choosing an adequate configuration of the electric RF fields and a static magnetic field defining a quantization axis for the spin, arbitrary spin rotations can be realized.

According to Duckheim and Loss on Ref. [12] and Golovach et al. on Ref. [13], EDSR has the advantage that it can be integrated in gated nanostructures.

### 1.3 SPIN MEASUREMENT

With the current capabilities it is possible, although awkwardly, to measure spin the direction of a single electron via its (small) magnetic moment, i.e. its Bohr Magneton  $\mu_B$  —for spin polarizable systems, spin measurement involves an ensemble average of spins. Actually spin measurement in devices is more related the sense of effects caused by spin population accumulation in the sample than with the measurement of individual spins. A typical measurement process involves:

**INJECTION OF A SPIN POPULATION.** A *non-equilibrium* spin population could be created by a number of means, like *interband* absorption of circularly polarized light (one of the most efficient methods) or spin transport from a ferromagnet.

**LUMINESCENCE ANALYSIS.** Electronic spin can be measured by analyzing the luminescence generated by the recombination process of spin polarized electrons with holes, provided that the electronic spin relaxation time is not very short compared with the recombination time.

Apart from luminescence, other schemes for spin detection have been proposed. For instance, one of them is based on Pauli's Principle, which reduces the measurement of spin polarization to a charge or current measurement, requiring a single-charge electrometer (already available) and a switchable spin-filter tunnel barrier (see [Spintronic Devices](#) on [Section 1.5](#), page 9). As mentioned by [Awshalom et al.](#) on page 253 of Ref. [14], optical measurements are also possible via the Faraday Rotation effect.

#### 1.4 SPIN RELAXATION

##### *Single Spin Relaxation*

As commented above, the spin-coherence, or spin relaxation time, refers to the time the spin direction tends to remain after external control is removed, causing spins to decay to random directions. Electronic spin-coherence results long in metals and semiconductors (about a nanosecond), what makes these materials a promising framework for spin-based devices and applications, like spin-encoded information (see [Section 1.5](#) on page 9). This decaying can be understood as a result of spin-orbit coupling, that is, spin precession around time-varying magnetic fields. Because those magnetic fields vary randomly, after a short time the spin is precessing around a completely different direction.

The genesis of such random fields is varied, ranging from interactions of electron-spins with nuclei-spins, momentum scattering, and the so called Elliot-Yafet, Dyakonov-Perel, and Bir-Aronov-Pikus mechanisms.

The single (or few) spin relaxation time is more often called *spin decoherence*, to distinguish it from spin ensemble relaxation. It is important for applications in spin-based quantum-computing (see [Section 1.5](#) on page 9), where it is believed that individual spins should last for about  $10^5$  gate operations.

*Spin  
decoherence  
is for single  
(few) spins*

##### *Ensemble Spin Relaxation*

As mentioned by [Igor Žutić et al.](#) on Ref. [10], spin relaxation of a spin ensemble is typically described through two parameters,

SPIN RELAXATION TIME ( $T_1$ , Longitudinal time, or spin-lattice time).

Is the time it takes for the longitudinal magnetization to reach equilibrium, or equivalently, the time in which thermal equilibrium is reached between the spin population and the lattice, by means of phonon transference.

*Thermal  
equilibrium*

SPIN DEPHASING TIME ( $T_2$ , Transverse time, or decoherence time).

The spin ensemble is initially precessing in phase about the longi-

*Phase  
coherence*

tudinal field, but due to spatial and temporal fluctuations of the precessing frequencies an ensemble of transverse electron spins loses their phase.  $T_1$  is the time such loss takes to occur.

These parameters came from the phenomenological Bloch-Torrey equations for magnetization dynamics. But if a microscopic expression for  $T_1$  and  $T_2$  is desired, a density-matrix formulation of the magnetization dynamics is usually performed and then compared with the Bloch equations to obtain  $T_1$  and  $T_2$ .

As pointed out by Igor Žutić *et al.* in Ref. [10], it is customary that, for either small magnetic fields or when no matter the experimental set up, both times  $T_1$  and  $T_2$  are referred as a single symbol  $\tau_s$ . Moreover,  $T_1$  is more often used in theoretical calculations whereas experiments tend to measure  $T_2$ .

## 1.5 SPINTRONIC DEVICES

Semiconductor spintronics could be the base for a new generation of devices that combine standard microelectronics with spin effects, but first, in order to be able to write and extract information of such devices, one must have the capability to create a spin population, transport it across the device (through different materials), manipulate it, and detect it. Unfortunately, not all of these operations have been performed, and in some cases, there isn't a complete theoretical understanding of the details, and much research remains to be done. Current open problems on spin physics and spin technology are, for example,

- Enhancement of spin polarization on conventional and novel materials,
- Detection of spin coherence on nano-devices, like quantum dots and quantum wells,
- Enhancement of electron spin lifetimes,
- Transport of spin polarized carriers (electrons, holes, nuclei, and ions),
- All-electrical and all-optical spin control,
- Fast spin-polarization switching.

*This  
thesis*

Nevertheless, many devices have been proposed, and it is believed that they will possess singular advantages compared to conventional electronic devices, like non-volatility, high speed data processing, less power consumption, increased integration densities, and increased phase control of coherence on length and time scales larger than in conventional electronics. Some remarkable proposals include:

**GMR DEVICE.** The Giant Magneto Resistance (**GMR**) structure device consists of alternating ferromagnetic and nonmagnetic metal layers (ferromagnetic materials are permanently magnetic). In this structure, the electric resistance through the layers has abrupt variations, depending on the relative magnetization orientation of the ferromagnetic layers, which is controlled by a magnetic field parallel to the layers: for parallel relative magnetizations the resistance is small, but for anti-parallel ones it is very large. The abrupt change in resistance is used as a high sensitive detector of variable magnetic fields, and is used for instance in the read/write heads of current magnetic storage devices.

**SPIN-LED.** In the Spin Light-Emitting-Diode the recombination of spin-polarized carriers results in the emission of right or left circularly polarized light in the direction normal to the surface. Through polarization analysis of the resulting radiation it is possible to get quantitative measurements of the spin injection efficiency, so that this device has served more as a test bed instrument than a commercial product, mostly because its low-temperature and high-magnetic field requirements.

**FIELD-EFFECT SPIN TRANSISTOR.** In 1989, **Datta and Das** proposed the first spintronic device. Its structure made of indium-aluminium-arsenide and indium-gallium-arsenide provides a channel for electron transport between two ferromagnetic electrodes. One of them acts as an *emitter electrode* and the other as a *collector electrode*, in analogy to the source and drain in a conventional electronic field-effect transistor. The operation is as follows: the emitter sends electrons with their spins oriented along the direction of the electrodes magnetization, while the collector (with the same electrode magnetization) acts as a *spin filter*, accepting electrons that have the same spin. A *gate electrode* applies a field that causes the electron spins to precess, thus acting as a modulator of the electronic current that can pass the spin filter. This proposal is known as the Datta-Das device, but it is yet to be realized because of the technical difficulties concerning clean spin control and injection from ferromagnetic sources. See Refs. [15] and [10].

*Spin filter*

*Datta-Das device*

**ALL-METAL SPIN TRANSISTOR.** It was proposed by **Johnson** (Ref. [16]) and consists of a 3-layered structure: a nonmagnetic metallic layer sandwiched between 2 ferromagnetic layers, being similar in structure and function to the GMR device. In this device the non-metallic layer acts as the *base*, one of the ferromagnetic layers as the *collector* and the other as the *emitter*; a battery is included in the *control circuit* (emitter-base) and the *direction* of the current in the *control circuit* (base-collector) is switched by changing the

*Spin-Switch  
Spin-Valve*

magnetization of the collector layer. This device acts as a spin valve or a switch, that is, it neither amplifies the current nor the voltage. See Ref. [16].

**SPINTRONIC SOLAR CELLS.** This proposal by [Das Sarma](#) plans to direct circular polarized solar light, coming from a filter, to a PN semiconductor junction of type III-V. This will create spin polarized electron-hole pairs in the *depletion layer*<sup>7</sup>, but because of the semiconductor type, the spin polarization will only be retained by electrons. The internal electric field in the depletion zone will cause that the holes move through the P side and the electrons to the N side. If this junction is connected to a circuit, then a spin polarized current will flow. See Ref. [7]

**SPIN-BASED QUANTUM COMPUTERS.** There are many proposals for quantum computing, and the Spin-Based Quantum Computer is one of them. Nevertheless, all these are long term projects because of tough technical difficulties, like coherence control. The spin-based proposal aims to use the natural property of spin-up or spin-down of electrons as the new binary units of processing, called *qubits*, which will be not restricted to represent just zeroes or ones, but an arbitrary superposition of them. Basically, to perform a computation, an initial state is imposed on the spins, and then they is allowed to evolve through a process of entanglement, which is a quantum property of correlation between spins, even though they are spatially separated.

[David P. Di Vincenzo](#), an IBM's researcher, states that to realize a quantum computer [spintronic or not] a set of 5+2 requirements must be fulfilled (see Ref. [17]), namely

1. A scalable physical system with well characterized qubits,
2. The ability to initialize the state of the qubits to a simple fiducial [reference] state, such as  $|000 \dots 0\rangle$ ,
3. Long relevant coherence times, much longer than the gate operation time,
4. A universal set of quantum gates,
5. A qubit specific measurement capability,
6. The ability to interconnect stationary and flying qubits, and
7. The ability to faithfully transmit flying qubits between specified locations.

5+2  
Quantum  
Computing  
Requirements

<sup>7</sup> The depletion layer is formed from a conducting region by removal of all free charge carriers, leaving none to carry a current. It is formed, for example, in the interface of a N-P junction.

The first five requirements are meant to serve for *quantum computation* (prime factoring and code-breaking crypto-systems are two ambitious problems aimed to be solved with it) and the last two requirements are needed to connect quantum computation to *quantum information processing* (at present, there are commercial cryptographic systems based on quantum cryptography) and some other operations require both quantum computation and quantum information (like the computation with input data dotted through many parties).

Because quantum computation requires a long coherence and fine control of quantum states, nuclear and electronic spins can function as qubits. Some particular proposals for spin-based quantum computers include:

**QUANTUM DOTS.** In this scheme the spin of a *single* electron trapped in a *quantum dot* is used as qubit, then an array of quantum dots is allowed to interact to form an entanglement of qubits. The individual electrons are manipulated with magnetic fields, and this is precisely one of the difficulties of this scheme: the individual manipulation of electrons. Another issue is the trapping of a single electron in a quantum dot, but recently it has been shown that an odd number of electrons trapped in a quantum dot could serve as a qubit (instead of only one). The problem of the disturbance caused on neighbor qubits by the magnetic field is planned to be eliminated with *quantum error correction* techniques.

**PHOSPHORUS NUCLEI ON SILICON.** This scheme was proposed by Kane (See Ref. [18]), where phosphorus atoms doped in a silicon substrate act as qubits. Each phosphorus nucleus transmits its spin to its electrons, which serve for single qubit operations. Two-qubit like operations are performed with electron-nucleus and electron-electron interactions.

*In brief*

Spintronic devices represent a great promise of improvement in current technology, and hundreds of scientists and engineers work around the world to solve the respective theoretical and practical drawbacks.

## 1.6 OBJECTIVES AND OVERVIEW OF THIS THESIS

The thesis work presented here is part of the research I performed under the supervision of Dr. Bernardo Mendoza during my Master in Science studies at Centro de Investigaciones en Óptica, A.C. (León, México).



Its main objectives are (1) to investigate the well known fact that the optical electron spin-injection on bulk semiconductors is affected by the application of stress, and (2) to explore the possibility of modulate such phenomenon by either compressive or expansive stresses. For that matter, a simple and effective method to compute the spin injection as a function of stresses (or a related quantity) is proposed, considering both compressive and expansive stresses.

To address this project, first in this [Chapter 1](#) a review of the broad field of spintronics has been given, including some remarkable proposals for spin-devices. Then in [Chapter 2](#) the basic theory of electronic spin is presented, and is followed in [Chapter 3](#) by a description of the framework used to quantify the spin injection on bulk semiconductors. In the last third of the presentation, [Chapter 4](#), expressions of the preceding chapters are evaluated, taking the approach of density functional theory (DFT) and employing pseudopotential band structures based on the local density approximation (LDA). For this purpose almost solely, *free* software programs were used.

At the end of the chapter, the main objective of this thesis demonstrated, i.e. the fact that in principle, the tuning of the spin-injection and its enhancement are possible by means the application of stresses. Finally, in [Chapter 6](#) a review of the results and the corresponding conclusions are presented.



## ELECTRONIC SPIN

## 2.1 BASIC DEMONSTRATION OF SPIN EXISTENCE

The first and most basic demonstration of the spin existence was performed in Germany (1921) by Gerlach and Stern. Actually they showed (see Ref. [19]) the existence of the electron's magnetic moment due to its spin. Basically, the experimental set up is as follows: paramagnetic silver atoms contained in a furnace heated at high temperature are permitted to escape through a small opening. After propagating in straight line in the vacuum, a collimating slit selects those atoms whose velocity is parallel to a particular direction. The emerging collimated beam then traverses the gap of an electromagnet and then condenses on a plate.

*Stern-Gerlach  
Experiment*

The classic theory predicted a deflection of the beam, but instead they observed an split of the beam into two beams, which were deflected in opposite directions. This showed that atoms had different magnetic properties. When the two beams impact in the plate they form two spots, whose width is due to the dispersion of the velocities and the width of the slit.

This experiment proved that only certain permitted orientations were allowed, i.e. the angular momentum is quantized.

Other experimental evidences of spin existence are:

**FINE STRUCTURE OF ATOMIC SPECTRA.** When atomic spectra is observed in detail, each spectral line is actually composed of a finite number of lines, i.e. there are groups of atomic levels very closely spaced.

**THE ANOMALOUS ZEEMAN EFFECT.** In the *normal* Zeeman effect the atomic spectra of an atom splits into several lines when a magnetic external field is present. The Schrödinger theory predicts that such splitting must result in an odd number of spectral lines, but experimental evidence showed that spectral lines of atoms with *odd* atomic number  $Z$  (the number of protons, which uniquely identifies a chemical element) were split into an *even* number of sub-levels.

**HALF-INTEGRAL ANGULAR MOMENTA.** This problem is closely related to the Stern-Gerlach experiment, which suggests that half-integral values of the quantum number  $j$  exist, but it is in conflict

with the fact that the orbital angular momentum  $\ell$  can only be integral

**MAGNETIC PROPERTIES.** Many substances, like metallic ferromagnets such as iron, cobalt, and nickel, are magnetizable with an external magnetic field, and retain its magnetization after the field has been removed. This phenomena can only be explained with the concept of ferromagnetic *domains* and *spin* (see footnote 4 on page 5).

## 2.2 SPIN INCLUSION INTO THE QUANTUM THEORY

Schrödinger  
Equation

The time-dependent Schrödinger equation

$$i\hbar \frac{\partial \psi}{\partial t} = \left( -\frac{\hbar^2}{2m} \nabla^2 + V \right) \psi \quad (2.1)$$

describes quantumly the motion of an electron that is under the influence of a potential. Here the electron is a particle that possesses three degrees of freedom, corresponding to the  $x$ ,  $y$ , and  $z$  coordinates, therefore its wave function has dependence only as  $\psi(x, y, z)$ . In [Equation 2.1](#)  $i\hbar \partial/\partial t$  is the energy operator  $\hat{E}$ ,  $-\hbar^2/2m \nabla^2$  is the kinetic energy operator  $\hat{T}$ , and  $\hat{V}$  is the potential operator. With the Schrödinger approach to quantum mechanics it is possible to study *exactly* only the Hydrogen atom, which only possesses two particles: a proton and an electron. More complex atoms, like Helium (a 3-body problem) and the rest (many-body problems) require to make *mathematical* simplifications in order to obtain analytical solutions. Such simplified solutions which nevertheless explain adequately many observed quantum phenomena, are inadequate in many studies, like the fine details in atomic spectra (spectral lines that seem to be one, but are actually two or more closely spaced).

Because removing the preceding mathematical simplifications make it impossible to solve analytically the Schrödinger equation, it became imperative to review the physical assumptions done in such theory, in order to explain a number of inconsistencies (like those mentioned in [Section 2.1](#)). For example, among the most important missing effects in the Schrödinger formulation were relativistic kinematics (mass, time, and length variations due to velocity) and magnetic effects (the orbital electron around the nucleus represents a varying electric current, which induces magnetism).

Relativistic effects were first included by simple substitution of the relativistic energy in the Schrödinger theory ([de la Peña](#), p. 834 of Ref. [20]),

$$E^2 = m^2 c^4 + c^2 p^2 \quad (2.2)$$

leading to the Klein-Gordon equation; which for the free particle ( $V = 0$ ) it takes the form

$$\left(\nabla^2 - \frac{1}{c^2} \frac{\partial^2}{\partial t^2}\right) \psi - \frac{m^2 c^2}{\hbar^2} \psi = 0. \quad (2.3)$$

*Klein-Gordon  
Equation*

Although this formulation includes relativistic effects, it nevertheless requires the spin property to be included by hand; moreover, it also presents some inconsistencies in the particle density (caused by the second order temporal derivative), and solutions with negative energies as well.

To circumvent these problems, in 1930 Paul Dirac proposed to linearize the relativistic energy expression in Equation 2.2, i.e. to find a linear relationship between  $\hat{E}$  and  $\hat{p}$ , whose square satisfied the relativistic energy equation. This linearization did not remove the problem of negative energies, which now Dirac interpreted as energies of anti-particles.<sup>1</sup> Dirac's equation for the free particle has the form

$$i\hbar \frac{\partial \Psi}{\partial t} = \left(-i\hbar c \boldsymbol{\alpha} \cdot \nabla + mc^2 \boldsymbol{\beta}\right) \Psi, \quad (2.4)$$

*Dirac's  
Equation*

where  $\boldsymbol{\alpha}$  and  $\boldsymbol{\beta}$  are  $4 \times 4$  matrices that must be chosen to fulfill the relativity laws. Therefore, Dirac's equation gives a relativistic quantum mechanical description of the electron and leads naturally to a new characteristic of the electron, its spin.

### 2.3 PAULI'S DESCRIPTION OF SPIN

In between the discovery of the electron spin and the introduction of Dirac's equation, Pauli proposed to incorporate the spin characteristic into the Schrödinger theory by introducing a number of supplementary non-relativistic postulates, offering an electron theory much simpler than Dirac's theory, but which nevertheless provides excellent agreement with experimental evidence (see Cohen-Tannoudji et al., on p. 968 of Ref. [21]).

In academic texts, Pauli's equation may be usually written in two forms (de la Peña, Ref. [20]):

*Pauli's  
Equation*

$$i\hbar \frac{\partial \Psi}{\partial t} = \frac{\mathbf{P}^2}{2m} \Psi + \left(V - \hat{V}_{\text{coupling}}\right) \Psi, \quad (2.5a)$$

$$i\hbar \frac{\partial \Psi}{\partial t} = \hat{H}_0 \Psi + \frac{\mu_0}{\hbar} \mathbf{B} \cdot \left(\hat{\mathbf{L}} + 2\hat{\mathbf{S}}\right) \Psi, \quad (2.5b)$$

<sup>1</sup> Two years before this proposal, D. Anderson found for the first time the anti-electron, most commonly known as positron.

where the interaction/coupling term between the external magnetic moment  $\mathbf{B}$  and the intrinsic magnetic moment  $\hat{\boldsymbol{\mu}}$  (associated to spin) is given by

$$\hat{V}_{\text{coupling}} = -\hat{\boldsymbol{\mu}} \cdot \mathbf{B} = \mu_0 \hat{\boldsymbol{\sigma}} \cdot \mathbf{B} = \frac{e\hbar}{2mc} \hat{\boldsymbol{\sigma}} \cdot \mathbf{B}, \quad (2.6)$$

with  $\mu_0$  as the Bohr's magneton  $\mu_{\text{Bohr}} = \hbar e/2m_e$  and  $\hat{\boldsymbol{\sigma}}$  as the Pauli's matrices (see [Equation 3.66](#) on page 35).

The Hamiltonian  $H_0 = P^2/2m$  in [Equation 2.5](#) is written in terms of the electron's *Canonical Momentum*  $\mathbf{p}_{\text{can}}$  due to its motion and due to the influence of an external magnetic field

$$\mathbf{p}_{\text{can}} = \mathbf{P}_{\text{kinetic}} + \frac{e}{c}\mathbf{A}, \quad (2.7)$$

where  $\mathbf{P}_{\text{kinetic}} = m\mathbf{v}$  is the *mechanical/kinetic momentum* and  $\mathbf{A}$  is the magnetic vector potential.

Therefore, for an electron that is influenced by an external magnetic field, the kinetic momentum operator is written as

$$\hat{\mathbf{P}}_{\text{kinetic}} = \hat{\mathbf{p}}_{\text{can}} - \frac{e}{c}\mathbf{A}. \quad (2.8)$$

In [Equation 2.5b](#),  $\mathbf{L}$  is the orbital angular momentum,  $\mathbf{s}$  is the intrinsic (spin) angular momentum, and  $\mathbf{J} = \mathbf{L} + \mathbf{S}$  is the total angular momentum.

## 2.4 PAULI'S POSTULATES

As axiomatically pointed out by [Cohen-Tannoudji et al.](#) in Ref. [21], the Pauli's postulates that lead to the preceding [Equation 2.5](#) are:

1. The spin operator  $\mathbf{S}$  is an angular momentum. Therefore, its three components are observables which cyclically satisfy the commutation relations

$$[S_x, S_y] = i\hbar S_z. \quad (2.9)$$

2. The spin operators act in a new space, the *spin state space*  $\mathcal{E}_s$ , where  $\mathbf{S}^2$  and  $S_z$  constitute a *complete set of commuting observables* (CSCO).
3. The state space  $\mathcal{E}$  of the particle being considered is the tensor product of the orbital state space  $\mathcal{E}_r$  and the spin state space  $\mathcal{E}_s$ :

$$\mathcal{E} = \mathcal{E}_r \otimes \mathcal{E}_s. \quad (2.10)$$

Consequently, all spin observables commute with all orbital observables.

4. The electron is a spin- $\frac{1}{2}$  particle ( $s = \frac{1}{2}$ ) and its intrinsic magnetic moment is given by

$$M_S = 2 \frac{\mu_B}{\hbar} S. \quad (2.11)$$

Therefore, the electronic spin state space  $\mathcal{E}_s$  is two dimensional.

*In brief*

Before the 1920's quantum theory could not explain a number of experimental evidences. Then researchers realized that it was required to include a new quantum property associated to the electron's spin around itself. Such quantity, known as quantum spin, was included *ad hoc* into Schrödinger theory with the adoption of the Pauli's Principles, and lately it was shown that spin arose from a more complete description given by Dirac, where relativistic effects were taken into consideration.





Part II

THEORY



### 3.1 INTRODUCTION

The purpose of this chapter is to show the key steps to derive an expression to quantify the degree of spin polarization (DSP) in bulk semiconductors. This polarization is carried out by absorption of circular polarized light, which causes electrons (1) to be promoted from the valence to the conduction band<sup>1</sup> and (2) to be optically oriented by the transference of angular momentum from photons to the electrons; the orientation of the electron spin is parallel or anti-parallel to the beam. The presentation of this chapter follows Nastos et al. as in Ref. [1].

The computation of the band structure, required to describe the optical spin injection, is made within the density functional theory (DFT, see Refs. [22] and [23]). These band structure calculations are restricted to the local density approximation (LDA), which is an approximation to the exchange-correlation energy functional in the DFT. The external perturbation is taken to come from a laser beam, and the Hamiltonian for the perturbation is written as

$$H_{\text{ext}} = -er^{\alpha}E^{\alpha}(t), \quad (3.1)$$

where  $e$  is the electric charge,  $r$  is the position operator,  $E(t)$  is the electric field of the applied beam. The Roman superscripts indicate Cartesian coordinates, that, when repeated as in Equation 3.1, mean that the coordinates are to be summed over. The intraband matrix elements that describe the change of state along the same band do not take part in the quantification of the spin polarization, therefore they are isolated from the interband matrix elements. The latter describe electron's change of states that include transition between different bands.

### 3.2 DENSITY-MATRIX EQUATION OF MOTION

The spin polarization can be quantified through the *spin injection rate*, which in turn can be computed by a Fermi golden rule derivation.

<sup>1</sup> ISOLATED ATOMS possess what are known as *quantum states*, each of them characterized by a set of quantum numbers and an energy level. For an isolated atom the energy levels are *discrete*. The atom's electrons always tend to be at the lowest energy level, one electron per quantum state. For a CONDENSATE OF ATOMS, like a crystal, each state of each atom becomes a state of the crystal, and the energies become spread over certain continuous bands. That results in the formation of allowed and forbidden bands.

Nevertheless, such approach is not suitable to take into account the excited coherences that emerge in noncentrosymmetric semiconductors (i.e., those lacking of inversion symmetry), where the conduction bands are spin-split by amounts smaller than the laser width, causing the laser beam to excite a coherent superposition of two conduction bands.

A more rigorous approach is to use a density-matrix single-particle description, where atoms are assumed to have only one electron, procedure that permits to include excited coherences consistently.

The equation of motion is

$$\begin{aligned} \frac{d}{dt} \rho_{mn}(\mathbf{k}; t) &= -i\hat{\omega}_{mn}(\mathbf{k})\rho_{mn}(\mathbf{k}; t) \\ &\quad - \frac{i}{\hbar} ([H^{\text{ext}}(t), \rho(\mathbf{k}; t)])_{mn}, \end{aligned} \quad (3.2)$$

where the commutator matrix elements are

$$\begin{aligned} ([H^{\text{ext}}(t), \rho(\mathbf{k}; t)])_{mn} &= \sum_p H_{mp}^{\text{ext}}(t) \rho_{pn}(\mathbf{k}; t) \\ &\quad - \sum_p H_{mp}^{\text{ext}}(t) \rho_{pn}(\mathbf{k}; t), \end{aligned} \quad (3.3)$$

and loss and dephasing are taken into account in

$$\hat{\omega}_{mn}(\mathbf{k}) = \omega_{mn} - i\Gamma_{mn}, \quad (3.4)$$

with  $\Gamma_{mn}$  being positive and small, and

$$\omega_{mn} \equiv \omega_c(\mathbf{k}) - \omega_v(\mathbf{k}). \quad (3.5)$$

Equation 3.3 can be solved assuming the presence of excited coherences, that is, the simultaneous excitation of two close bands,  $c$  and  $c'$ , by the energy width of the laser beam (see Figure 1).

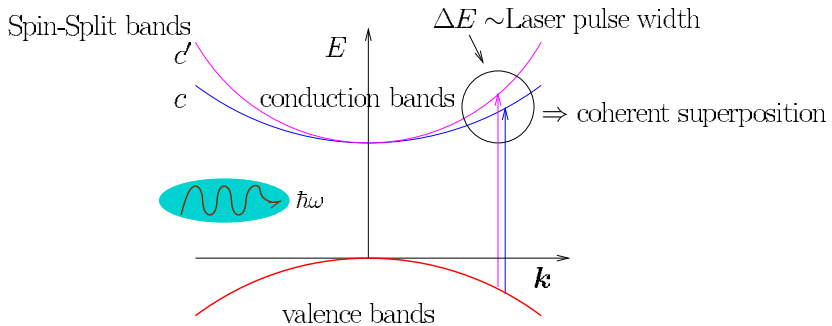


Figure 1: (color online). Coherence arise from simultaneous excitation of two close conduction bands,  $c$  and  $c'$ , by the finite energy width of the laser beam.

## 3.3 MULTI-SCALE SOLUTION OF THE EQUATION OF MOTION

Multiple-scale analysis is a general perturbation framework that is useful in systems characterized by different time scales (see [Kevorkian and Cole](#) on Ref. [24]). For the problem at hand, [Equation 3.2](#), the method allows the separation of the pulse time, the carrier cycle, and the dephasing and loss times. The interest is in the response to a continuous wave field of the form

$$\mathbf{E}(t) = \mathbf{E}_{\text{env}}(t)e^{-i\omega t} + \mathbf{E}_{\text{env}}^*(t)e^{i\omega t} \quad (3.6)$$

where the amplitude  $\mathbf{E}_{\text{env}}(t)$  is called the *slowly varying envelope function*. To implement the multiple scales treatment a new variable is defined

$$\tau = \omega t \quad (3.7)$$

and then the preceding equations are re-defined in terms of  $\tau$ :

$$\frac{d}{d\tau} \rho_{mn}(\tau) = -i \frac{\hat{\omega}_{mn}(\mathbf{k})}{\omega} \rho_{mn}(\tau) - \frac{i}{\hbar\omega} ([\mathbf{H}^{\text{ext}}(\tau), \rho(\tau)])_{mn}, \quad (3.8)$$

$$\mathbf{H}_{\text{ext}}(\tau) = -e r^{\alpha} \mathbf{E}^{\alpha}(\tau), \quad (3.9)$$

$$\mathbf{E}(\tau) = \mathbf{E}_{\text{env}}(\tau)e^{-i\omega\tau} + \mathbf{E}_{\text{env}}^*(\tau)e^{i\omega\tau}. \quad (3.10)$$

Since the intraband matrix elements of  $r_{mn}^{\alpha}$  do not contribute to the spin injection in the conduction band, they are neglected from the beginning. To introduce the different time scales, the preceding functions are explicitly written in terms of two new variables:  $\tau_0$  and  $\tau$

$$\tau_0 = \tau \quad \text{and} \quad (3.11a)$$

$$\tau_1 = \eta\tau \quad \text{with} \quad \eta \ll 1, \quad (3.11b)$$

That is,  $\tau_0$  describes faster phenomena than  $\tau_1$ . Notice that the functions depending on these new variables vary significantly only as  $\tau$  and  $\tau_0$  range over unity; therefore the *slowly varying envelope function* is written as

$$\mathbf{E}(\tau) = \mathbf{E}_{\text{env}}(\tau_1)e^{-i\omega\tau_0} + \mathbf{E}_{\text{env}}^*(\tau_1)e^{i\omega\tau_0}. \quad (3.12)$$

As pointed out above, multiple scale analysis is a perturbative method and the solution to [Equation 3.8](#) is proposed as

$$\rho_{mn}(\tau) = \sum_{u=-\infty}^{\infty} e^{-iu\tau_0} \rho_{mn;u}(\tau), \quad (3.13)$$

where the  $u$ 's are integers. Inserting Equation 3.13 into Equation 3.8, we write the equation of motion as,

$$\begin{aligned} \frac{d}{d\tau} \rho_{mn;u}(\tau) = & -i \left( \frac{\hat{\omega}_{mn}}{\omega} - u \right) \rho_{mn;u}(\tau) \\ & + i\eta \left[ \sigma_{mp}(\tau_1) \rho_{pn;(u-1)}(\tau) \right. \\ & \quad + \bar{\sigma}_{mp}(\tau_1) \rho_{pn;(u+1)}(\tau) \\ & \quad - \rho_{mp;(u-1)}(\tau) \sigma_{pn}(\tau_1) \\ & \quad \left. - \rho_{mp;(u+1)}(\tau) \bar{\sigma}_{pn}(\tau_1) \right] \end{aligned} \quad (3.14)$$

where the  $\sigma$  terms, which are dimensionless, are defined as

$$\eta \sigma_{mp}(\tau_1) \equiv \frac{e r_{mp}^a E^a(\tau_1)}{\hbar \omega} \quad \text{and} \quad (3.15a)$$

$$\eta \bar{\sigma}_{mp}(\tau_1) \equiv \frac{e r_{mp}^a E^{a*}(\tau_1)}{\hbar \omega}. \quad (3.15b)$$

Now a perturbative solution in powers of  $\rho$  of Equation 3.14 is proposed,

$$\rho_{mn;u}(\tau) = \rho_{mn;u}^{(0)}(\tau_1) + \eta \rho_{mn;u}^{(1)}(\tau_1) + \eta^2 \rho_{mn;u}^{(2)}(\tau_1) + \dots \quad (3.16)$$

Defining

$$\left( \frac{\hat{\omega}_{mn}}{\omega} - u \right) \rightarrow C_{mn;u} = C_{mn;u}^{(0)} + \eta C_{mn;u}^{(1)} \quad (3.17)$$

and assuming that due to damping, for a given  $(mnu)$  both  $C_{mn;u}^{(0)}$  and  $C_{mn;u}^{(1)}$  will not be nonzero, that is, only one survives for a given  $(mnu)$ . (see Figure 2).

Now a set of equations can be constructed from Equation 3.14, one for each power of  $\eta$ , if

$$\frac{\partial}{\partial \tau} = \frac{\partial}{\partial \tau_0} + \eta \frac{\partial}{\partial \tau_1} + \dots \quad (3.18)$$

The proposed solution in Equation 3.16 sets all time dependence at the  $\tau_1$ -level (slow time), therefore, from now the sub-index '1' is dropped. For further simplicity, all time dependence is left out. With these conventions

$$\text{for } \eta^0 : C_{mn;u}^{(0)} \rho_{mn;u}^{(0)} = 0, \quad (3.19)$$

$$\begin{aligned} \text{for } \eta^{i+1} : \frac{\partial}{\partial \tau} \rho_{mn;u}^{(i)} = & -i C_{mn;u}^{(0)} \rho_{mn;u}^{(i+1)} - i C_{mn;u}^{(1)} \rho_{mn;u}^{(i)} \\ & + i D_{mn;u}^{(i)}, \end{aligned} \quad (3.20)$$

where

$$\begin{aligned}
 D_{mn;u}^{(i)} &= \sum_p \left( \sigma_{mp} \rho_{pn;(u-1)}^{(i)} + \bar{\sigma}_{mp} \rho_{pn;(u+1)}^{(i)} \right) \\
 &- \sum_p \left( \rho_{mp;(u-1)}^{(i)} \sigma_{pn} + \rho_{mp;(u+1)}^{(i)} \bar{\sigma}_{pn} \right). \quad (3.21)
 \end{aligned}$$

Now we separate the terms for which  $C_{mn;u}^{(0)} = 0$  from those for which  $C_{mn;u}^{(0)} \neq 0$  (called *allowed* and *forbidden* terms, respectively. See Figure 2).

$$\rho_{mn;u}^{(i)} = \begin{cases} \alpha_{mn;u}^{(i)} & \text{if } C_{mn;u}^{(0)} = 0 \text{ allowed} \\ \beta_{mn;u}^{(i)} & \text{if } C_{mn;u}^{(0)} \neq 0 \text{ forbidden} \end{cases} \quad (3.22)$$

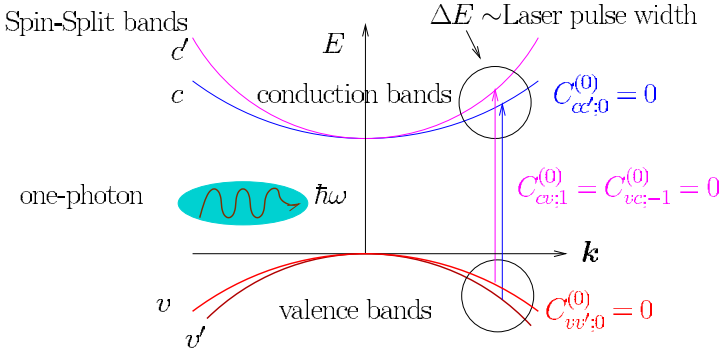


Figure 2: (color online) Diagrammatic representation of the *allowed* and the *forbidden* terms of Equation 3.22. It is assumed that due to damping, for a given  $(mnu)$  both  $C_{mn;u}^{(0)}$  and  $C_{mn;u}^{(1)}$  will not be nonzero, that is, only one survives for a given  $(mnu)$

From Equation 3.19

$$\beta_{mn;u}^{(0)} = 0, \quad (3.23)$$

that is, the only components  $\rho_{mn;u}^{(0)}$  that survive are the allowed terms. The  $i = 0$  term of Equation 3.20 with  $u = 0$  gives

$$\frac{\partial}{\partial \tau} \alpha_{mn;u}^{(0)} = -iC_{mn;u}^{(1)} \alpha_{mn;u}^{(0)} + ia_{mn;u} \mathcal{A}_{mn;u}^{(0)} \quad (3.24)$$

$$\beta_{mn;u}^{(1)} = \frac{b_{mn;u} \mathcal{A}_{mn;u}^{(0)}}{C_{mn;u}^{(0)}} \quad (3.25)$$

where

$$\begin{aligned} A_{mn;u}^{(i)} &= \sum_P \left( \sigma_{mp} \alpha_{pn;(u-1)}^{(i)} + \bar{\sigma}_{mp} \alpha_{pn;(u+1)}^{(i)} \right) \\ &\quad - \sum_P \left( \alpha_{mp;(u-1)}^{(i)} \sigma_{pn} + \alpha_{mp;(u+1)}^{(i)} \bar{\sigma}_{pn} \right) \end{aligned} \quad (3.26)$$

and

$$a_{mn;u} = 1 \quad \text{and} \quad b_{mn;u} = 0 \quad \text{if} \quad C_{mn;u}^{(0)} = 0,$$

$$a_{mn;u} = 0 \quad \text{and} \quad b_{mn;u} = 1 \quad \text{if} \quad C_{mn;u}^{(0)} \neq 0.$$

For the problem at hand, there are two sets of levels for the  $(mn)$  pairs: the conduction bands ( $cc'$ ) and the valence bands ( $vv'$ ). As bands of the same kind (conduction or valence) are supposed to be close to each other

$$C_{cc';0}^{(0)} = 0 \quad \text{and} \quad C_{cc';-1}^{(0)} = 0, \quad (3.27a)$$

and as in this problem only one-photon processes are considered

$$C_{cv;1}^{(0)} = 0 \quad \text{and} \quad C_{vc;-1}^{(0)} = 0. \quad (3.27b)$$

The rest of the  $C_{mn;u}^{(0)}$  are nonzero; therefore,

$$\alpha_{cv;1}^{(0)}, \quad \alpha_{vc;-1}^{(0)}, \quad \alpha_{cc';0}^{(0)} \quad \text{and} \quad \alpha_{vv';0}^{(0)} \neq 0. \quad (3.27c)$$

Collecting terms from [Equation 3.24](#) and dropping the superscript  $(0)$

$$i \frac{\partial \alpha_{cv;1}}{\partial \tau} = C_{cv;1}^{(1)} \alpha_{vc;1} - \sum_{v'} \sigma_{cv'} \alpha_{v'v;0} + \sum_{c'} \alpha_{cc';0} \sigma_{c'v}, \quad (3.28a)$$

$$i \frac{\partial \alpha_{vc;-1}}{\partial \tau} = C_{vc;-1}^{(1)} \alpha_{vc;-1} - \sum_{c'} \bar{\sigma}_{vc'} \alpha_{c'c;0} + \sum_{v'} \alpha_{vv';0} \bar{\sigma}_{v'c}, \quad (3.28b)$$

$$i \frac{\partial \alpha_{cc';0}}{\partial \tau} = C_{cc';0}^{(1)} \alpha_{cc';0} - \sum_v (\sigma_{cv} \alpha_{vc';-1} - \alpha_{cv;1} \bar{\sigma}_{vc'}), \quad (3.28c)$$

$$i \frac{\partial \alpha_{vv';0}}{\partial \tau} = C_{vv';0}^{(1)} \alpha_{vv';0} - \sum_c (\bar{\sigma}_{vc} \alpha_{cv';1} - \alpha_{vc;-1} \sigma_{cv'}). \quad (3.28d)$$

These equations are said to derive full excitation and saturation of the upper levels.

### 3.3.1 Perturbative Solution

Equations [3.28](#) can be solved by a perturbative approach. For instance, by setting

$$\alpha_{vv';0} \approx \delta_{vv'}, \quad (3.29)$$



throughout the time integration of Equation 3.28d and solving approximately Equations (3.28a), (3.28b), and (3.28c) for  $\alpha_{cv;1}$ ,  $\alpha_{vc;-1}$ , and  $\alpha_{cc';0}$ . Such a process gives

$$i \frac{\partial \alpha_{cv;1}}{\partial \tau} \approx C_{cv;1}^{(1)} \alpha_{vc;1} - \sigma_{cv} \quad \text{and} \quad (3.30)$$

$$i \frac{\partial \alpha_{vc;-1}}{\partial \tau} \approx C_{vc;-1}^{(1)} \alpha_{vc;-1} + \bar{\sigma}_{vc}. \quad (3.31)$$

The last equation has the form

$$\frac{dy}{dx} + p(x)y = q(x), \quad (3.32)$$

which is a linear equation whose solution can be obtained by the application of an integrating factor  $\mu$ , as follows

$$y = \mu^{-1}(x) \int dx' \mu(x') q(x') + c, \quad \text{with} \quad \mu(x) = e^{\int dx' p(x')}. \quad (3.33)$$

Now, assuming that  $\tau$  is much longer than the damping and dephasing times and that  $E_{\text{env}}$  is nearly constant, one gets

$$\begin{aligned} \alpha_{cv;1} &= e^{-iC_{cv;1}^{(1)}\tau} \int_0^\tau d\tau' [i\sigma_{cv}(\tau')] e^{iC_{cv;1}^{(1)}\tau'} \\ &\approx \frac{\sigma_{cv}}{C_{cv;1}^{(1)}} (1 - e^{-iC_{cv;1}^{(1)}\tau}) \\ &\approx \frac{\sigma_{cv}}{C_{cv;1}^{(1)}} \quad \text{for} \quad \tau \gg 1. \end{aligned} \quad (3.34)$$

Similarly

$$\alpha_{vc;-1} \approx -\frac{\bar{\sigma}_{vc}}{C_{vc;-1}^{(1)}} \quad \text{for} \quad \tau \gg 1. \quad (3.35)$$

Substituting Equation 3.34 and Equation 3.35 into Equation 3.28c one gets

$$\frac{\partial \alpha_{cc';0}}{\partial \tau} = -iC_{cc';0}^{(1)} \alpha_{cc';0} + \frac{1}{i} \sum_v \left( \frac{\sigma_{cv} \bar{\sigma}_{vc'}}{C_{vc';-1}^{(1)}} + \frac{\sigma_{cv} \bar{\sigma}_{vc'}}{C_{cv;1}^{(1)}} \right), \quad (3.36)$$

where

$$C_{cv;1}^{(1)} = -\frac{1}{\eta\omega} (\omega - \omega_{cv} + i\gamma_{cv}) \quad \text{and} \quad (3.37a)$$

$$C_{vc';-1}^{(1)} = \frac{1}{\eta\omega} (\omega - \omega_{c'v} - i\gamma_{vc'}). \quad (3.37b)$$

The time dependence can be inserted back with the substitution

$$\frac{\partial}{\partial \tau_1} \rightarrow \frac{1}{\eta\omega} \frac{\partial}{\partial t'} \quad (3.38)$$

and the variable of interest, the density matrix, is placed instead of  $\alpha$ ,

$$\alpha_{cc';0} \rightarrow \rho_{cc'}, \quad (3.39)$$

and the loss and dephasing implied in  $\gamma$  are expressed clearly as being small by writing  $\gamma$  as a small number  $\epsilon$ ,

$$\gamma \rightarrow \epsilon. \quad (3.40)$$

All these considerations give

$$\begin{aligned} \frac{\partial \rho_{cc'}}{\partial t} &= -i(\omega_{cc'} - i\epsilon) \rho_{cc'} - \frac{e^2 E^a(\omega) E^{b*}(\omega)}{i\hbar^2} \\ &\times \sum_{\nu} r_{c\nu}^a r_{\nu c'}^b \left( \frac{1}{\omega - \omega_{c'\nu} - i\epsilon} - \frac{1}{\omega - \omega_{c\nu} + i\epsilon} \right). \end{aligned} \quad (3.41)$$

It remains to solve Equation 3.42 for  $\rho_{cc'}$ .

$$\begin{aligned} \frac{\partial \rho_{cc'}}{\partial t} &= -i(\omega_{cc'} - i\epsilon) \rho_{cc'} + \frac{e^2 E^a(\omega) E^{b*}(\omega)}{i\hbar^2} \\ &\times \sum_{\nu} r_{c\nu}^a r_{\nu c'}^b \left( \frac{1}{\omega - \omega_{c'\nu} - i\epsilon} - \frac{1}{\omega - \omega_{c\nu} + i\epsilon} \right). \end{aligned} \quad (3.42)$$

In order to proceed further, we take  $\epsilon \rightarrow 0$  in the first term, and then we change the density matrix operator to the so called *interaction representation*, which requires the following replacement

$$\hat{\rho} \longrightarrow \tilde{\rho} = e^{iH_0 t/\hbar} \hat{\rho} e^{-iH_0 t/\hbar}, \quad (3.43)$$

with  $H_0$  the ground state Hamiltonian. The matrix elements are now,

$$\begin{aligned} \langle c\mathbf{k} | \tilde{\rho} | c'\mathbf{k} \rangle &= \langle c\mathbf{k} | e^{iH_0 t/\hbar} \hat{\rho} e^{-iH_0 t/\hbar} | c'\mathbf{k} \rangle \\ &= e^{i\omega_c t} \langle c\mathbf{k} | \hat{\rho} | c'\mathbf{k} \rangle e^{-i\omega_{c'} t} \\ \tilde{\rho}_{cc'}(\mathbf{k}) &= e^{i\omega_{cc'} t} \rho_{cc'}(\mathbf{k}), \end{aligned} \quad (3.44)$$

where we used  $H_0 |n\mathbf{k}\rangle = \hbar\omega_n(\mathbf{k}) |n\mathbf{k}\rangle$  with  $\hbar\omega_n(\mathbf{k})$  the energy of the electronic band  $n$  at point  $\mathbf{k}$ , and  $|n\mathbf{k}\rangle$  the Bloch state. The reciprocal lattice vector  $\mathbf{k}$  is restricted to the irreducible part of the first Brillouin zone. From Eq. (3.44) the time derivative of  $\tilde{\rho}_{cc'}(\mathbf{k})$  is given by

$$\begin{aligned} \frac{d\tilde{\rho}_{cc'}(\mathbf{k})}{dt} &= \left( i\omega_{cc'} \rho_{cc'}(\mathbf{k}) + \frac{\partial \rho_{cc'}(\mathbf{k})}{\partial t} \right) e^{i\omega_{cc'} t} \\ &= \frac{e^2 E^a(\omega) E^{b*}(\omega)}{i\hbar^2} e^{i\omega_{cc'} t} \\ &\times \sum_{\nu} r_{c\nu}^a r_{\nu c'}^b \left( \frac{1}{\omega - \omega_{c'\nu} - i\epsilon} - \frac{1}{\omega - \omega_{c\nu} + i\epsilon} \right), \end{aligned} \quad (3.45)$$

where we used Eq. (3.42), and the  $\epsilon \rightarrow 0$  still needs to be taken.

Within the density matrix formalism, the expectation value of an observable  $\mathcal{O}$  is given by

$$\mathcal{O} = \text{Tr}(\widehat{\rho}\widehat{\mathcal{O}}), \quad (3.46)$$

where  $\text{Tr}$  denotes the trace, given by the sum over the diagonal matrix elements, and  $\widehat{\mathcal{O}}$  is the quantum mechanical operator associated to the observable  $\mathcal{O}$ . Then,

$$\begin{aligned} \mathcal{O} &= \int \frac{d^3\mathbf{k}}{8\pi^3} \sum_c \langle c\mathbf{k}|\widehat{\rho}\widehat{\mathcal{O}}|c\mathbf{k}\rangle = \int \frac{d^3\mathbf{k}}{8\pi^3} \sum_{cc'} \langle c\mathbf{k}|\widehat{\rho}|c'\mathbf{k}\rangle \langle c'\mathbf{k}|\widehat{\mathcal{O}}|c\mathbf{k}\rangle \\ &= \int \frac{d^3\mathbf{k}}{8\pi^3} \sum_{cc'} \rho_{cc'}(\mathbf{k}) \mathcal{O}_{c'c}(\mathbf{k}), \end{aligned} \quad (3.47)$$

where we used the closure relationship  $\sum_c |c\mathbf{k}\rangle \langle c\mathbf{k}| = 1$ . In the interaction picture,  $\widetilde{\mathcal{O}}_{c'c} = \langle c'\mathbf{k}| e^{iH_0 t/\hbar} \widehat{\mathcal{O}} e^{-iH_0 t/\hbar} |c\mathbf{k}\rangle = \mathcal{O}_{c'c} e^{-i\omega_{cc'} t}$  and thus we can also write

$$\mathcal{O} = \int \frac{d^3\mathbf{k}}{8\pi^3} \sum_{cc'} \widetilde{\rho}_{cc'}(\mathbf{k}) \widetilde{\mathcal{O}}_{c'c}(\mathbf{k}), \quad (3.48)$$

and so, we can calculate the expectation value using  $\widehat{\rho}$  and  $\widehat{\mathcal{O}}$  in either the standard Schrödinger representation or the interaction representation. From the previous equation, the rate of change of  $\mathcal{O}$  is given by

$$\begin{aligned} \frac{d\mathcal{O}}{dt} &= \int \frac{d^3\mathbf{k}}{8\pi^3} \sum_{cc'} \frac{d\widetilde{\rho}_{cc'}(\mathbf{k})}{dt} \widetilde{\mathcal{O}}_{c'c}(\mathbf{k}) \\ &= \frac{e^2}{i\hbar^2} \int \frac{d^3\mathbf{k}}{8\pi^3} \sum_{vcc'} \widehat{\mathcal{O}}_{c'c} r_{cv}^a r_{vc'}^b \left( \frac{1}{\omega - \omega_{c'v} - i\epsilon} - \frac{1}{\omega - \omega_{cv} + i\epsilon} \right) \\ &\quad E^a(\omega) E^{b*}(\omega), \end{aligned} \quad (3.49)$$

where we used Eq. (3.45), and we notice that the  $e^{i\omega_{cc'} t}$  and  $e^{-i\omega_{cc'} t}$  factor cancel each other.

### 3.4 DEGREE OF SPIN POLARIZATION

Equation 3.49 can be used to compute the *spin-injection rate*  $\dot{\mathcal{S}} \equiv d\mathcal{S}/dt$  with

$$\widehat{\mathcal{O}} \rightarrow \widehat{\mathcal{S}}^a = \frac{\hbar}{2} \widehat{\sigma}^a \quad (3.50)$$

where  $\widehat{\sigma}^a$  are the Pauli Matrices

$$\widehat{\sigma}^x = \begin{pmatrix} 0 & 1 \\ 1 & 0 \end{pmatrix}, \quad \widehat{\sigma}^y = \begin{pmatrix} 0 & -i \\ i & 0 \end{pmatrix}, \quad \text{and} \quad \widehat{\sigma}^z = \begin{pmatrix} 1 & 0 \\ 0 & -1 \end{pmatrix} \quad (3.51)$$

that are operators in spinor space, therefore,

$$\begin{aligned} \frac{d}{dt} \mathcal{S}^a &= \frac{e^2}{i\hbar^2} \int \frac{d^3\mathbf{k}}{8\pi^3} \sum_{vcc'} \widehat{\mathcal{S}}_{c'c}^a r_{cv}^b r_{vc'}^c \\ &\quad \left( \frac{1}{\omega - \omega_{c'v} - i\epsilon} - \frac{1}{\omega - \omega_{cv} + i\epsilon} \right) \\ &\quad \mathbb{E}^b(\omega) \mathbb{E}^{c*}(\omega). \end{aligned} \quad (3.52)$$

Using the so called time-reversal invariance, as described by [Lax](#) on Ref. [25] and [Najmaie et al.](#) on Ref. [8], by which

$$\omega_{\mathbf{m}}(-\mathbf{k}) = \omega_{\mathbf{k}}, \quad (3.53a)$$

$$r_{\mathbf{m}\mathbf{n}}^a(-\mathbf{k}) = r_{\mathbf{n}\mathbf{m}}^a(\mathbf{k}), \quad \text{and} \quad (3.53b)$$

$$\mathcal{S}_{\mathbf{m}\mathbf{n}}^a(-\mathbf{k}) = -\mathcal{S}_{\mathbf{n}\mathbf{m}}^a(\mathbf{k}), \quad (3.53c)$$

we can add the  $\mathbf{k}$  and  $-\mathbf{k}$  contributions to the integral in Eq. (3.54) to obtain

$$\begin{aligned} \frac{d\mathcal{S}^a}{dt} &= \frac{e^2}{i\hbar^2} \int_{\mathbf{k}>0} \frac{d^3\mathbf{k}}{8\pi^3} \sum_{vcc'} \left[ \left( \mathcal{S}_{c'c}^a r_{cv}^b r_{vc'}^c \right) \Big|_{\mathbf{k}} + \left( \mathcal{S}_{c'c}^a r_{cv}^b r_{vc'}^c \right) \Big|_{-\mathbf{k}} \right] \\ &\quad \times \left( \frac{1}{\omega - \omega_{c'v} - i\epsilon} - \frac{1}{\omega - \omega_{cv} + i\epsilon} \right) \mathbb{E}^b \mathbb{E}^{c*} \\ &= \frac{e^2}{i\hbar^2} \int_{\mathbf{k}>0} \frac{d^3\mathbf{k}}{8\pi^3} \sum_{vcc'} \left[ \left( \mathcal{S}_{c'c}^a r_{cv}^b r_{vc'}^c \right) \Big|_{\mathbf{k}} - \left( \widehat{\mathcal{S}}_{cc'}^a r_{vc}^b r_{c'v}^c \right) \Big|_{\mathbf{k}} \right] \\ &\quad \times \left( \frac{1}{\omega - \omega_{c'v} - i\epsilon} - \frac{1}{\omega - \omega_{cv} + i\epsilon} \right) \mathbb{E}^b \mathbb{E}^{c*} \\ &= \frac{e^2}{i\hbar^2} \frac{1}{2} \int \frac{d^3\mathbf{k}}{8\pi^3} \sum_{vcc'} \left[ \left( \mathcal{S}_{c'c}^a r_{cv}^b r_{vc'}^c \right) - \left( \widehat{\mathcal{S}}_{c'c}^a r_{cv}^b r_{vc'}^c \right)^* \right] \\ &\quad \times \left( \frac{1}{\omega - \omega_{c'v} - i\epsilon} - \frac{1}{\omega - \omega_{cv} + i\epsilon} \right) \mathbb{E}^b \mathbb{E}^{c*} \\ &= \frac{e^2}{\hbar^2} \int \frac{d^3\mathbf{k}}{8\pi^3} \sum_{vcc'} \text{Im} \left[ \mathcal{S}_{c'c}^a r_{cv}^b r_{vc'}^c \right] \\ &\quad \times \left( \frac{1}{\omega - \omega_{c'v} - i\epsilon} - \frac{1}{\omega - \omega_{cv} + i\epsilon} \right) \mathbb{E}^b \mathbb{E}^{c*}, \end{aligned} \quad (3.54)$$

where in going from the second to the third equal sign, we use the fact that for any Hermitian operator  $\mathcal{O}_{\mathbf{m}\mathbf{n}}(\mathbf{k}) = \mathcal{O}_{\mathbf{n}\mathbf{m}}^*(\mathbf{k})$ , and that the one half comes from the unrestricted integration over all values of  $\mathbf{k}$  and not only  $\mathbf{k} > 0$ . Aided by the identity

$$\lim_{\epsilon \rightarrow 0} \frac{1}{\omega - \omega_{cv} - i\epsilon} = \mathcal{P}(\omega - \omega_{cv}) + i\pi\delta(\omega - \omega_{cv}), \quad (3.55)$$

where  $\mathcal{P}$  means the *principal part*, Eq. (3.54) can be written as

$$\begin{aligned}
\frac{dS^a}{dt} &= \frac{e^2}{\hbar^2} \int \frac{d^3k}{8\pi^3} \sum_{vcc'} \text{Im} [S_{c'c}^a r_{cv}^b r_{vc'}^c] \left\{ \mathcal{P} \left( \frac{1}{\omega - \omega_{c'v}} - \frac{1}{\omega - \omega_{cv}} \right) \right. \\
&\quad \left. + i\pi [\delta(\omega - \omega_{c'v}) + \delta(\omega - \omega_{cv})] \right\} E^b E^{c*} \\
&= \frac{e^2}{\hbar^2} \int \frac{d^3k}{8\pi^3} \sum_{vcc'} \text{Im} [S_{c'c}^a r_{cv}^b r_{vc'}^c] \left\{ \mathcal{P} \left( \frac{\omega_{c'c}}{(\omega - \omega_{c'v})(\omega - \omega_{cv})} \right) \right. \\
&\quad \left. + i\pi [\delta(\omega - \omega_{c'v}) + \delta(\omega - \omega_{cv})] \right\} E^b E^{c*} \\
\frac{dS^a}{dt} &\simeq \frac{i\pi e^2}{\hbar^2} \int \frac{d^3k}{8\pi^3} \sum'_{vcc'} \text{Im} (S_{c'c}^a r_{cv}^b r_{vc'}^c) \\
&\quad [\delta(\omega - \omega_{c'v}) + \delta(\omega - \omega_{cv})] E^b E^{c*}, \tag{3.56}
\end{aligned}$$

since the term that goes with the principal part is of the order of  $\omega_{cc'}$  which is very small as the states  $c$  and  $c'$  are quasi degenerate. Indeed, the primed sigma symbol  $\sum'$  means that the sum is to be performed on pairs  $cc'$  of quasi-degenerate conduction bands. It seems that in Equation 3.63 there are two resonant frequencies, one at  $\omega = \omega_{cv}(\mathbf{k})$  and other at  $\omega = \omega_{c'v}(\mathbf{k})$ , but actually there is only one. This can be shown if one changes  $c \rightleftharpoons c'$  in the second  $\delta$  function, then

$$\begin{aligned}
\frac{dS^a}{dt} &= \frac{i\pi e^2}{\hbar^2} \int \frac{d^3k}{8\pi^3} \sum'_{vcc'} \left( \text{Im} [S_{c'c}^a r_{cv}^b r_{vc'}^c] + \text{Im} [S_{cc'}^a r_{c'v}^b r_{vc}^c] \right) \\
&\quad \delta(\omega - \omega_{cv}) E^b E^{c*}, \tag{3.57}
\end{aligned}$$

where it is clear that the only resonant frequency is at  $\omega = \omega_{cv}(\mathbf{k})$ . Moreover, the coherence of the  $v \rightarrow c$  and  $v \rightarrow c'$  processes is given by the addition of the two imaginary  $\text{Im}()$  terms that are proportional to the probability of such transitions. Compactly time rate of  $S^a$  is written as,

$$\frac{dS^a}{dt} = \tilde{\zeta}^{abc} E^b(\omega) E^{c*}(\omega), \tag{3.58}$$

where

$$\begin{aligned}
\tilde{\zeta}^{abc} &= \frac{i\pi e^2}{\hbar^2} \int \frac{d^3k}{8\pi^3} \sum'_{vcc'} \left( \text{Im} [S_{c'c}^a r_{cv}^b r_{vc'}^c] + \text{Im} [S_{cc'}^a r_{c'v}^b r_{vc}^c] \right) \\
&\quad \delta(\omega - \omega_{cv}), \tag{3.59}
\end{aligned}$$

is denoted as the *spin-injection 3<sup>th</sup> rank pseudo-tensor component*<sup>2</sup>, which, in the argot of nonlinear optics, plays a similar role than the 2<sup>th</sup> order

<sup>2</sup> In simple terms, a pseudo-tensor is an object that transforms like a tensor under a proper rotation, but changes sign under an improper rotation. That is, a pseudo-tensor is a transformation that can be expressed as an inversion followed by a proper rotation.

susceptibility  $\chi^{abc}$ . We see that  $\zeta^{abc}$  is purely imaginary and that  $\zeta^{abc} = -\zeta^{acb}$ , since

$$\begin{aligned}
& 2i \left( \text{Im} [\mathcal{S}_{c'c}^a r_{cv}^b r_{vc'}^c] + \text{Im} [\mathcal{S}_{cc'}^a r_{c'v}^b r_{vc}^c] \right) \\
&= \mathcal{S}_{c'c}^a r_{cv}^b r_{vc'}^c - \left( \mathcal{S}_{c'c}^a r_{cv}^b r_{vc'}^c \right)^* \\
&\quad + \mathcal{S}_{cc'}^a r_{c'v}^b r_{vc}^c - \left( \mathcal{S}_{cc'}^a r_{c'v}^b r_{vc}^c \right)^* \\
&= \mathcal{S}_{c'c}^a r_{cv}^b r_{vc'}^c - \mathcal{S}_{cc'}^a r_{vc}^b r_{c'v}^c + \mathcal{S}_{cc'}^a r_{c'v}^b r_{vc}^c - \mathcal{S}_{c'c}^a r_{vc}^b r_{c'v}^c \\
&= -\mathcal{S}_{cc'}^a r_{vc}^b r_{c'v}^c + \mathcal{S}_{cc'}^a r_{c'v}^b r_{vc}^c - \mathcal{S}_{c'c}^a r_{vc}^b r_{c'v}^c + \mathcal{S}_{c'c}^a r_{c'v}^b r_{vc}^c \\
&= -2i \left( \text{Im} [\mathcal{S}_{cc'}^a r_{vc}^b r_{c'v}^c] + \text{Im} [\mathcal{S}_{c'c}^a r_{vc}^b r_{c'v}^c] \right) \\
&= -2i \left( \text{Im} [\mathcal{S}_{c'c}^a r_{cv}^b r_{vc'}^c] + \text{Im} [\mathcal{S}_{cc'}^a r_{c'v}^b r_{vc}^c] \right). \tag{3.60}
\end{aligned}$$

Now, from [Equation 3.70](#) we have that

$$\begin{aligned}
\frac{d\mathcal{S}^a}{dt} &= \tilde{\zeta}^{abc} E^b E^{c*} + \tilde{\zeta}^{acb} E^c E^{b*} && \text{no sum over } b \neq c \\
&= \tilde{\zeta}^{abc} E^b E^{c*} - \tilde{\zeta}^{abc} E^c E^{b*} && \text{no sum over } b \neq c \\
&= \tilde{\zeta}^{abc} \left( E^b E^{c*} - E^c E^{b*} \right) && \text{no sum over } b \neq c \\
&= -2i \tilde{\zeta}^{abc} \text{Im} [E^{b*} E^c] && \text{no sum over } b \neq c. \tag{3.61}
\end{aligned}$$

Writing  $\tilde{\zeta}^{abc} = i\zeta^{abc}$ , we finally obtain, as we must,

$$\frac{d\mathcal{S}^a}{dt} = 2\zeta^{abc} \text{Im} [E^{b*} E^c], \tag{3.62}$$

as a real quantity, with

$$\begin{aligned}
\zeta^{abc} &= \frac{\pi e^2}{\hbar^2} \int \frac{d^3k}{8\pi^3} \sum'_{vcc'} \left( \text{Im} [\mathcal{S}_{c'c}^a r_{cv}^b r_{vc'}^c] + \text{Im} [\mathcal{S}_{cc'}^a r_{c'v}^b r_{vc}^c] \right) \\
&\quad \delta(\omega - \omega_{cv}), \tag{3.63}
\end{aligned}$$

For the purposes of this work, bands that are separated from each other by less than 30 meV are considered as quasi-degenerate, which is approximately both the laser pulse energy and the room temperature energy (see [Figure 1](#)).

### 3.5 DEGREE OF SPIN POLARIZATION

[Equation 3.42](#) can be used to compute the *spin-injection rate*  $\dot{\mathcal{S}} \equiv d\mathcal{S}/dt$  with

$$\dot{\mathcal{S}} = \text{Tr} \left( \dot{\rho} \hat{\mathcal{S}} \right) \quad \text{or} \quad \dot{\mathcal{S}}^a = \text{Tr} \left( \dot{\rho} \hat{\mathcal{S}}^a \right), \tag{3.64}$$

where

$$\hat{\mathbf{S}} = \frac{\hbar}{2} \boldsymbol{\sigma} \quad \text{or} \quad \hat{\mathbf{S}}^a = \frac{\hbar}{2} \sigma^a \quad (3.65)$$

and  $\sigma^a$  are the Pauli Matrices

$$\sigma^x = \begin{pmatrix} 0 & 1 \\ 1 & 0 \end{pmatrix}, \quad \sigma^y = \begin{pmatrix} 0 & -i \\ i & 0 \end{pmatrix}, \quad \text{and} \quad \sigma^z = \begin{pmatrix} 1 & 0 \\ 0 & -1 \end{pmatrix}. \quad (3.66)$$

Aided by the identity

$$\frac{1}{\omega - \omega_{c\nu} - i\epsilon} = \mathcal{P}(\omega - \omega_{c\nu}) + i\pi \delta(\omega - \omega_{c\nu}), \quad (3.67)$$

where  $\mathcal{P}$  means the *principal part*, the spin injection rate can be found combining the preceding equations, giving

$$\begin{aligned} \frac{d}{dt} S^a &= \frac{\pi e^2}{\hbar^2} \left\{ \sum'_{cc'\nu} \int \frac{d^3\mathbf{k}}{8\pi^3} S_{c'c}^a(\mathbf{k}) r_{\nu c'}^b(\mathbf{k}) r_{c\nu}^c(\mathbf{k}) \right. \\ &\quad \left. [\delta(\omega_{c\nu}(\mathbf{k}) - \omega) + \delta(\omega_{c'\nu}(\mathbf{k}) - \omega)] \right\} \\ &\quad E^b(-\omega) E^c(\omega). \end{aligned} \quad (3.68)$$

The primed sigma symbol  $\sum'$  means that the sum is to be performed on pairs  $cc'$  of quasi-degenerate conduction bands. It seems that in [Equation 3.68](#) there are two resonant frequencies, one at  $\omega = \omega_{c\nu}(\mathbf{k})$  and other at  $\omega = \omega_{c'\nu}(\mathbf{k})$ , but actually there is only one. This can be shown if one changes  $c \rightleftharpoons c'$  in the second  $\delta$  function, then

$$\begin{aligned} \frac{d}{dt} S^a &= \frac{\pi e^2}{\hbar^2} \left\{ \sum_{cc'\nu\mathbf{k}} \left[ S_{cc'}^a(\mathbf{k}) r_{c\nu}^b(\mathbf{k}) r_{\nu c'}^c(\mathbf{k}) + S_{c'c}^a(\mathbf{k}) r_{c'\nu}^b(\mathbf{k}) r_{\nu c}^c(\mathbf{k}) \right] \right. \\ &\quad \left. \delta(\omega - \omega_{c\nu}(\mathbf{k})) \right\} E^b(-\omega) E^c(\omega), \end{aligned} \quad (3.69)$$

where it is clear that the only resonant frequency is at  $\omega = \omega_{c\nu}(\mathbf{k})$ . The  $(-\omega)$  argument refers to the complex conjugate of the field in the frequency domain. The term in curly braces is a 3<sup>th</sup> rank pseudo-tensor<sup>3</sup>, and is denoted as the *spin-injection pseudo-tensor component*  $\zeta^{abc}$ , which, in the argot of nonlinear optics, plays a similar role than the 2<sup>th</sup> order susceptibility  $\chi^{abc}$ . Compactly  $\hat{\mathbf{S}}$  is written as,

$$\frac{d}{dt} S^a = \zeta^{abc} E^b(-\omega) E^c(\omega) \quad (3.70)$$

$$\begin{aligned} \zeta^{abc}(\omega) &= \frac{\pi e^2}{\hbar^2} \sum_{cc'\nu\mathbf{k}} \left[ S_{cc'}^a(\mathbf{k}) r_{c\nu}^b(\mathbf{k}) r_{\nu c'}^c(\mathbf{k}) + S_{c'c}^a(\mathbf{k}) r_{c'\nu}^b(\mathbf{k}) r_{\nu c}^c(\mathbf{k}) \right] \\ &\quad \delta(\omega - \omega_{c\nu}(\mathbf{k})). \end{aligned} \quad (3.71)$$

<sup>3</sup> In simple terms, a pseudo-tensor is an object that transforms like a tensor under a proper rotation, but changes sign under an improper rotation. That is, a pseudo-tensor is a transformation that can be expressed as an inversion followed by a proper rotation.

For the purposes of this work, bands that are separated from each other by less than 30 meV are considered as quasi-degenerate, which is approximately both the laser pulse energy and the room temperature energy (see [Figure 1](#)).

The *spin injection rate*  $\dot{\mathcal{S}}$  and *spin-injection pseudo-tensor component*  $\zeta^{abc}$  describe the *total* spin injected to the conduction band. Albeit by themselves, they don't describe clearly if large values of them correspond to the injection of few electrons with high alignment to the beam direction, or just many electrons poorly spin polarized. For this reason it is necessary to describe the spin polarization as an average of the electron spin, i.e., as the rate of the spin injection rate  $\dot{\mathcal{S}}$  respect to the [total] *carrier injection rate*  $\dot{n}$ , i.e.

$$\text{DSP}^a = \frac{2}{\hbar} \frac{\dot{\mathcal{S}}^a}{\dot{n}} \quad (3.72)$$

The DSP is measured along the light propagation vector, specified by the Roman superscript  $a$ . Either a multiple scale analysis or a Fermi Golden Rule derivation gives for the carrier injection rate,  $\dot{n} \equiv dn/dt$ ,

$$\begin{aligned} \dot{n} &= \frac{2\pi e^2}{\hbar^2} \int \sum_{cv} \frac{d^3k}{8\pi^3} r_{vc}^a(\mathbf{k}) r_{cv}^b(\mathbf{k}) \delta[\omega_{cv}(\mathbf{k}) - \omega] \\ &\quad \times E^a(-\omega) E^b(\omega) \end{aligned} \quad (3.73)$$

where the same connotation as in [Equation 3.70](#) applies for the  $(-\omega)$  argument. The term in curly braces is identified as the *carrier-injection tensor component*  $\xi^{ab}$ , that is,

$$\dot{n} = \xi^{ab} E^a(-\omega) E^b(\omega) \quad (3.74)$$

$$\xi^{ab} = \frac{2\pi e^2}{\hbar^2} \int \sum_{cv} \frac{d^3k}{8\pi^3} r_{vc}^a(\mathbf{k}) r_{cv}^b(\mathbf{k}) \delta[\omega_{cv}(\mathbf{k}) - \omega]. \quad (3.75)$$

*In brief*

Equations (3.70) to (3.75) represent the main results of this chapter. In Part II, [Chapter 4](#), they are evaluated to compute the DSP of two bulk semiconductors, gallium arsenide and silicon, firstly under normal conditions, and then for the cases that compressive and expansive stress are applied. It is shown that DSP can be enhanced by the application of stress.



## STRESS MODULATION OF DSP ON BULK SEMICONDUCTORS

---

### 4.1 OBJECTIVES

As pointed out in [Chapter 1, Section 1.6](#), the aim of this thesis is to show that the Degree of Spin Polarization (DSP) in bulk semiconductors can be modulated, and even enhanced, by the application of compressive or expansive stress.

### 4.2 COMPUTATIONAL APPROACH

In [Chapter 3](#) it was shown that the DSP in a cold and clean bulk semiconductor<sup>1</sup> is described by

$$\text{DSP}^a = \frac{2}{\hbar} \frac{\dot{S}^a}{\dot{n}}, \quad (4.1a)$$

$$\dot{S}^a = \zeta^{abc}(\omega) E^b(-\omega) E^c(\omega), \quad (4.1b)$$

$$\dot{n} = \xi^{ab} E^a(-\omega) E^b(\omega), \quad (4.1c)$$

$$\zeta^{abc}(\omega) = \frac{\pi e^2}{\hbar^2} \sum_{cc'vk} \left[ S_{cc'}^a(\mathbf{k}) r_{cv}^b(\mathbf{k}) r_{vc'}^c(\mathbf{k}) + S_{c'c}^a(\mathbf{k}) r_{c'v}^b(\mathbf{k}) r_{vc}^c(\mathbf{k}) \right] \delta(\omega - \omega_{cv}(\mathbf{k})), \quad (4.1d)$$

$$\xi^{ab} = \frac{2\pi e^2}{\hbar^2} \int \sum_{cv} \frac{d^3k}{8\pi^3} r_{vc}^a(\mathbf{k}) r_{cv}^b(\mathbf{k}) \delta[\omega_{cv}(\mathbf{k}) - \omega]. \quad (4.1e)$$

$$\omega_{mn} \equiv \omega_c(\mathbf{k}) - \omega_v(\mathbf{k}). \quad (4.1f)$$

As mentioned on [Section 3.5](#), the DSP is measured along the light propagation vector, specified by the Roman superscript  $z$ . The frequencies of interest for the present work are optical frequencies, i.e. those in the energy range  $\hbar\omega$  from 0.5 to 4.5 eV ( $\nu$  in 120–1,090 THz). The first thing to do to evaluate expressions (4.1) is to obtain the position and spin matrix elements,  $r_{cv}^a(\mathbf{k})$  and  $S_{mn}^a(\mathbf{k})$  respectively,

$$S_{cm}^a(\mathbf{k}) \delta(\mathbf{k} - \mathbf{k}') = \langle c\mathbf{k} | \hat{S}^a | m\mathbf{k}' \rangle, \quad (4.2a)$$

$$r_{cv}^a(\mathbf{k}) = \frac{v_{cv}^a(\mathbf{k})}{i \omega_{cv}(\mathbf{k})}, \quad (4.2b)$$

$$v_{cv}^a(\mathbf{k}) \delta(\mathbf{k} - \mathbf{k}') = \langle c\mathbf{k} | \hat{v}^a | v\mathbf{k}' \rangle. \quad (4.2c)$$

<sup>1</sup> A cold semiconductor has all its electrons in the valence band.

4.2.1 *First-principles band structure computation*

The computation of the band structure from first-principles is used to evaluate the set of equations 4.1. In general, first-principles band structure computations enable to find the total energy of a system as a function of atomic positions only. Specifically it was employed the density-functional theory (DFT) within the local density approximation (LDA) as well as pseudo-potentials.

*The density-functional theory*

DFT

The DFT, attributed to Hohenberg and Kohn (1964) (Ref. [26]), is a strict formulation of the general many-body problem in which the basic idea is that the dependence on the external potential  $V(\mathbf{r})$  is replaced by a dependence on the density distribution of charge  $n(\mathbf{r})$ . The key idea behind the DFT is that *the total energy of a system*

- is a *unique* functional of the density-charge  $n(\mathbf{r})$ , and that
- the functional is minimal for the correct density.

DFT requires two approximations

Nevertheless, the direct application of DFT requires to approximate both the kinetic and the exchange-correlation energies, giving poor agreement with experiments.

Non-interacting system

Kohn-Sham equations

**KINETIC ENERGY APPROXIMATION:** A year later, in 1965, Kohn and Sham (Ref. [27]), instead of approximating the contribution of the kinetic energy, proposed to introduce a conceptual auxiliary non-interacting system that reproduces the charge density of the interacting system. There, the ground state of the non-interacting system is given by a set of Schrödinger-like equations, the Kohn-Sham equations, that are to be solved self-consistently.

Concept of Self-consistency

The self-consistent field method (SCF) (see the review by Blinder on Ref. [28]) has its origins in the Hartree-Fock model of the atom. SCF method implies to solve a set of equations, one equation for each particle (the electrons, in this thesis), taking into account the influence of all other  $N - 1$  particles, by means of a *mean-field* that represents such  $N - 1$  particles. The equations are solved numerically, generally by iterative fixed-point algorithms (see the review by Payne et al. on Ref. [29]).

**EXCHANGE-CORRELATION APPROXIMATION:** The remaining approximation, that to the energy from the exchange-correlation interactions between electrons, is done via *exchange-correlation functionals*. A number of such functionals exists, but the one employed in this thesis is the *local-density approximation (LDA)*. In this approximation, the contribution to the exchange-correlation energy from a

LDA

point in space  $r_i$  is taken as that from a uniform electron-gas at some appropriate density for that point in space  $r_i$ .

#### *Further reading on DFT*

The subject of first-principles computations is rich and complex. General references to the DFT include that of Jones and Gunnarsson on Ref. [23] and the succinct and short review by Argaman on Ref. [22]. A tiny but effective description of first-principles electronic structure calculations is given in Sec. III-V of Ref. [30] by A. Mujica et al. A general reference for electronic structure theory is the book by Martin, Ref. [31]. Actual numerical techniques are given by Payne et al. on Ref. [29]; also useful is the online tutorial of the ABINIT Software at [www.abinit.org](http://www.abinit.org). A succinct review of the self-consistency field (SCF) method is given by Blinder on Ref. [28].

#### 4.2.2 Computational implementation: The Abinit Software

The first-principles band structure computation is implemented with the aid of the *free* software ABINIT<sup>2</sup> developed by Gonze et al. (Ref. [32]). This program computes, from *ab-initio* principles, material properties such as the total energy, charge density, and electronic structure of systems made of electrons and nuclei, using pseudo-potentials and planewave basis within the DFT formalism, as well as excited states by the Time-Dependent-DFT or within Many-Body Perturbation Theory.

In this way, the DSP for a given semiconductor structure can be systematically computed, provided that one knows essential parameters of the material, like the unitary cell geometry, the number of atoms in the unitary cell, the primitive translation vectors defining the crystal, etc. Such values are fed to ABINIT to compute the spin and position matrix elements (Equation 4.2a and Equation 4.2b).

In the examples worked out in this thesis (see Section 5.2 and Section 5.3), the pseudopotential calculations were done as described by Nastos et al. on Ref. [1]. The momentum matrix elements were calculated as described by Mendoza et al. on Ref. [2].

Because LDA band structure computations underestimate the band gap of insulators (see Jones and Gunnarsson on Ref. [23]), a *scissors-correction* was applied. It consists of a rigidly upward shift in energy of all conduction bands by an amount that corrects the LDA estimation.

#### 4.2.3 Integration on the Brillouin Zone

Once the position and spin matrix elements,  $r_{cv}^a(\mathbf{k})$  and  $S_{mn}^a(\mathbf{k})$ , have been computed, the *spin-injection pseudo-tensor components*  $\zeta^{abc}(\omega)$

<sup>2</sup> Visit [www.abinit.org](http://www.abinit.org).

(Equation 4.1d) and the *carrier-injection tensor components*  $\xi^{ab}$  (Equation 4.1e) remain to be determined. To do so, one takes advantage of the fact that both equations have the form

$$G(\omega) = \sum_{cv} G_{cv}(\omega) \quad (4.3)$$

with

$$G_{cv}(\omega) = \int \frac{d^3\mathbf{k}}{8\pi^3} g_{cv}(\mathbf{k}) \delta[\omega - \omega_{cv}(\mathbf{k})]. \quad (4.4)$$

This sort of integral is known as *Joint-Density of States Integrals* (JDOS-

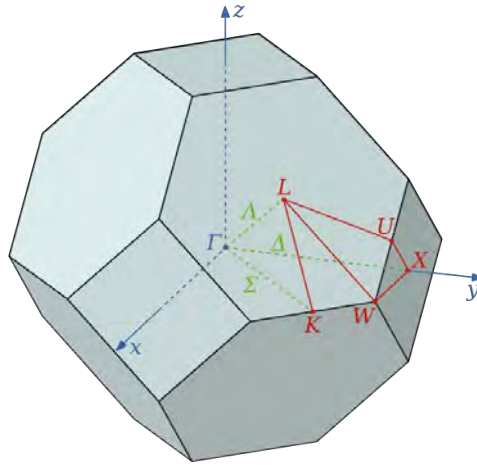


Figure 3: (color online) The first Brillouin Zone (BZ) is a uniquely defined primitive cell of the reciprocal lattice in the frequency domain. The image shows the high symmetry lines and points. The former definition and the image were taken from <http://en.wikipedia.org>; they are licensed to be used under the Gnu Public License.

JDOS  
Integrals

Integrals), where the  $\delta$  function effectively reduces the 3-dimensional integral over the Brillouin Zone (BZ, see Figure 3) to a 2-dimensional integral on the surface given by

$$\omega_{cv}(\mathbf{k}) = \omega \quad (\text{Integration Surface, within the BZ}). \quad (4.5)$$

These JDOS-Integrals can be evaluated by simple sampling on  $\mathbf{k}$ , nevertheless, because of the usual complexity of both the crystal semiconductors and the constant-energy surface-integrals, is preferable to calculate them by the so-called linearized analytic tetrahedron method (LATM).

### The LATM Integration Method

The evaluation of JDOS's by the LATM requires to perform the following steps (refer to Equation 4.3 and Equation 4.4):

1. Break up the BZ volume into tetrahedra (triangular pyramids having four plane triangular faces). This is called the tetrahedral grid.
2. Evaluate and store the integrand factor  $g_{cv}(\mathbf{k})$  and the energy eigenvalues  $\hbar\omega_m(\mathbf{k})$  at every tetrahedron vertex,
3. For each energy  $\omega$ , identify inside each tetrahedron the constant-energy surface  $\omega_{cv}(\mathbf{k}) = \omega$  (defined by the  $\delta$  function). By the knowledge of the energy at each vertex (step 2), find by linear interpolation the energies within the tetrahedra.
4. Evaluate analytically the surface integral in Equation 4.4. Use linear interpolation of the integrand  $g_{cv}(\mathbf{k})$  over the tetrahedron.
5. Finally, sum over the contributions of all tetrahedra to get  $G_{cv}(\omega)$ .

Linear  
Analytic  
Tetrahedral  
Method  
of Integration

People in Surface Optics Group at CIO, in collaboration with Nastos et al. (authors of Ref. [1]), have developed a FORTRAN subroutine to implement the LATM.

### 4.3 CONVERGENCE ANALYSIS

On band structure computations, apart from the model itself (DFT, GW<sup>3</sup>, etc.), there are some parameters that must be properly set, to a minimum or a maximum, in order to obtain good concordance between the computed signals and the experimental evidence. To find out the most adequate value, one must run at least several calculations at various values of them till one obtains [almost] the same response. This is called convergence analysis.

Convergence  
Analysis

For the problem at hand in this thesis, there are three of those parameters that significantly influence the results. They three must be set to a *minimal* value to get converged results (if they are set to a higher value the results are *almost* exactly the same, but the computational time increases largely). They are<sup>4</sup>:

NOTE: Words written in the typewriter font refer to variables or parameters in the computer programs, either ABINIT or TINIBA.

<sup>3</sup> GW calculations use a set of self-consistent equations for the one-electron Green's function to compute the self-energy of many-body systems. The approximation was first proposed by L. Hedin. See L. Hedin, Phys. Rev. 139, A 796 (1965).  
<sup>4</sup> See the ABINIT's documentation at [www.abinit.org](http://www.abinit.org).

NUMBER OF  $k$ -POINTS (`nkpt`). The number of  $k$ -points (number of  $k$  vectors) influences on the sampling of the BZ (see [Figure 3](#) on p. 40).

NUMBER OF CONDUCTION BANDS (`cband`). The number of conduction bands plus the number of valence bands, gives the total number of bands (`nband`), occupied or possibly unoccupied. For all them the wave-functions should be computed along with eigenvalues.

The semiconductors studied on this thesis, silicon and gallium arsenide, have both four valence bands.

ENERGY CUTOFF (`ecut`). Is a real parameter used for the kinetic energy cutoff. It controls the number of plane-waves at a given  $k$ -point by:

$$\frac{1}{2} [2\pi|\mathbf{k} + \mathbf{G}_{\max}|]^2 = \text{ecut} \quad (4.6)$$

All plane-waves inside this basis-sphere (centered at  $k$ ) are included in the basis. This parameter has a huge effect on the quality of a calculation; basically the larger `ecut`, the better convergence of the calculation. The units of `ecut` are units of energy; in `ABINIT` it is typically given in Hartrees (Ha), the energy unit in the Atomic Unit System<sup>5</sup> (roughly  $1 \text{ Ha} \approx 27.21 \text{ eV}$ ), but it can be given in other energy units.

#### 4.4 STRESS-INDUCED VOLUMETRIC CHANGE

As mentioned in [Section 1.6](#) (page 12), the main objective of this thesis is to investigate the possibility for the modulation of the optical electron spin-injection on bulk semiconductors, by the application of stresses, either compressive or expansive.

##### 4.4.1 Experimental realization

As pointed out in the review by [A. Mujica et al.](#) on Ref. [30] the techniques of high-pressure physics are highly developed. The employed devices mostly based on the diamond anvil cell (DAC), see [Figure 4](#), which has the important characteristic that applies very static high-pressures well above 100 GPa. The basic idea behind it is the same of all high-pressure devices: the application of a force to a small surface.

<sup>5</sup> There are 'two' Atomic Unit Systems, one of them measures energy in Hartree units and the other in Rydberg units. In both of them, the numerical values of the following six physical constants are all unity by definition: the electron's mass and charge; the Hydrogen's Bohr radius and its absolute value of the electric potential energy in the ground state; the Planck's constant  $h$ , and Coulomb's constant  $k$ .

This thesis

<sup>1</sup> Hartree is roughly 27.21 eV

This thesis

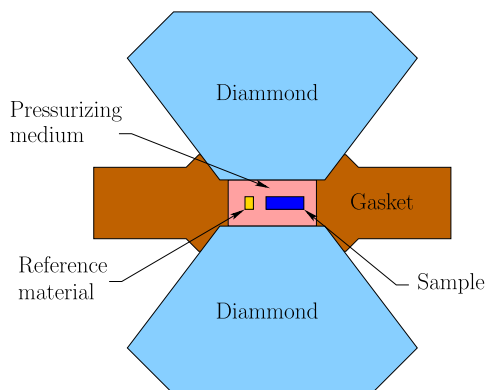


Figure 4: Schematic depiction of a diamond anvil cell (DAC), which is the basis of almost all high-pressure devices (the gasket is commonly a metallic foil). Because diamond is transparent on a wide energy range, DACs are adequate to study the sample via its radiation-matter properties (sketch reproduced from Ref. [30]).

In a DAC, the sample is placed between two diamonds, and the sample is normally immersed in a fluid contained in a *pressure chamber* into which the sample is placed. The chamber is normally filled with a fluid, in order to ensure quasi-hydrostatic and homogeneous conditions. Typical fluids in use are methanol-ethanol, silicon oils,  $N_2$ , Ar, and He. Special care must be taken because the fluid could undergo phase changes or produce complex diffraction patterns. To diminish this effects one can use cryogenic techniques.

The fact that diamond is transparent on frequencies that go from the near ultraviolet ( $\sim 5.5$  eV) to the infrared ( $\sim 10$  meV), including also a window at hard X-rays energy ( $>10$  keV), makes this device so attractive for the use of radiation to study the sample under such high-pressures.

Expansion experiments are mostly based on thermal expansions.

#### 4.4.2 Range of volumetric change

The application of large forces on a material can cause a *structural phase transition* in the material, that is, a sudden change in the arrangement of its atoms. Such phase transition can be caused by a continuous or discontinuous change; the important phenom is that a change in the crystal symmetry occurs. Moreover, the phase transition may be reversible or irreversible. Then a natural question arises: what are the adequate bounds of the volumetric compression (expansion) in order to avoid phase and structure changes?

*phase transition*

*What is the range of acceptable volumetric change?*

At a first look to the bibliography of High Pressure Physics, I found out about Prof. Stefan Turneure, from Washington State University.

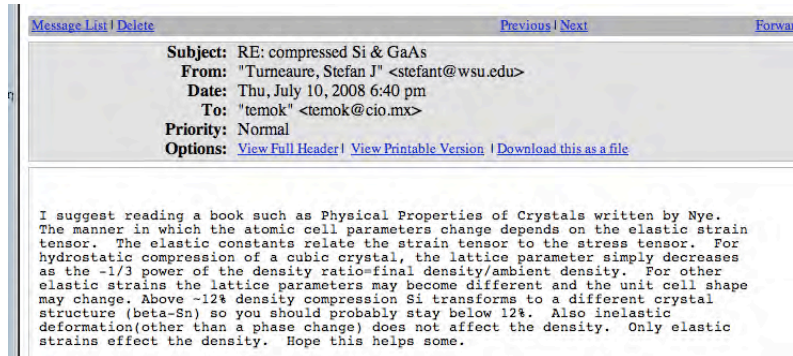


Figure 5: (color online) Prof. Turneure's e-mail (Researcher at Washington University). In his missive, he suggests me to stay below 12% of volumetric change compression for bulk silicon. In agreement with my advisor, Dr. Bernardo Mendoza, the computations on this thesis for both crystals were restricted to  $\pm 10\%$  of volumetric change.

He is author of many publications on the subject, one of them closely related to such bounds (Ref. [33]). Afterwards, I interchanged a couple of e-mails with him to get an advice. He kindly explained to me that (see Figure 5 on page 44) silicon suffers a structure change to  $\beta$ -Sn when it undergoes about 12% of density compression. As a general approach, and in agreement with my advisor, Dr. Bernardo Mendoza, the computations on this thesis for both crystals were restricted to  $\pm 10\%$  of volumetric change.

This  
thesis

#### 4.4.3 Numerical Implementation

To address that, the ratio of the volumetric change due to an applied stress was used as the independent-input-variable, that is, the volume variations quantify the amount of compression or expansion at the crystal structures studied in this thesis, bulk silicon and bulk gallium arsenide (see Section 5.2 and Section 5.3).

Independent  
input  
variable

Once the independent variable was defined, the next issue was how to indicate the **ABINIT** program to compute the spin and position matrix elements,  $r_{cv}^a(\mathbf{k})$  and  $S_{mn}^a(\mathbf{k})$  (Equation 4.2a and Equation 4.2b), for a crystal structure that has suffered a volumetric change. The answer lies in two fundamental concepts used in the study of crystalline structures (see pages 64 and 65 of Ashcroft and Mermin's textbook, Ref. [34]):

Key  
operational  
question

THE BRAVAIS LATTICE (3D) Are all points with position vectors  $\mathbf{R}$  of the form

$$\mathbf{R} = n_1 \mathbf{a}_1 + n_2 \mathbf{a}_2 + n_3 \mathbf{a}_3 \quad (4.7)$$



where  $n_1, n_2$ , and  $n_3$  range through all integral values, and  $\mathbf{a}_1, \mathbf{a}_2$ , and  $\mathbf{a}_3$  are any three non-coplanar vectors, called PRIMITIVE VECTORS, that are said to generate or span the lattice<sup>6</sup>.

PRIMITIVE (UNIT) CELL A volume in space that, when translated through all the vectors in a Bravais lattice, just fills out all the space without either overlapping itself or leaving voids. A primitive (unit) cell *must* contain precisely one lattice point. For a given set of primitive vectors, the corresponding primitive (unit) cell is the set of all points  $\mathbf{r}$  of the form

$$\mathbf{r} = x_1 \mathbf{a}_1 + x_2 \mathbf{a}_2 + x_3 \mathbf{a}_3 \quad x_i \in (0, 1) \quad (4.8)$$

As both concepts rely on the primitive vectors:

A variation in length of the primitive vectors induces a variation of both, the Bravais lattice and the unit cell.

*Key idea*

To induce such variation in **ABINIT** implies to vary the **ABINIT's** **acell** parameter, which stands for scAle CELL. It is a real triad **acell(1,2,3)** given in Bohr units<sup>7</sup> that acts as a length parameter. Essentially it gives the length scales that, when applied to the *dimensionless* Real space PRIMITIVE translation vectors (**rprim**, a  $3 \times 3$  unity matrix), gives the *dimensional* primitive vectors (**rprimd**),

*Key action*

*Concrete action*

$$\mathbf{rprimd}(i, j) = \mathbf{rprim}(i, j) \times \mathbf{acell}(j) \quad \text{for } i, j = 1, 2, 3 \\ \text{(i.e. } x, y, z \text{).} \quad (4.9)$$

*In brief*

The modulation of **DSP** via the application of either compressive or expansive stresses is obtained by setting the independent-variable as an hypothetical change in volume due to the application of the stress. To avoid phase and structural changes in the crystal, those variations are restricted to be in the  $\pm 10\%$  range.

Then **ABINIT** is instructed to compute the spin and matrix elements for a number of hypothetical volumetric variations. This is accomplished by varying the **ABINIT's** **acell** parameter in the mentioned range.

<sup>6</sup> Alternatively, the Bravais lattice is an infinite array of discrete points arranged in such manner that seem *absolutely* the same from whichever point the lattice is observed.

<sup>7</sup> [Atomic Units] One Bohr is roughly 0.53 Angstroms or  $53 \times 10^{-3}$  nm.



Part III

RESULTS AND CONCLUSIONS



## EXAMPLES OF DSP MODULATION

---

### 5.1 OBJECTIVES

The fact that the **DSP** response can be modulated by the application of either compressive or expansive stresses was already known.

In **Chapter 4**, a simple method to achieve such modulation was proposed, and in this chapter it is applied to study two important crystal semiconductors: bulk silicon and bulk gallium arsenide.

### 5.2 EXAMPLE 1. BULK SILICON STUDY

#### 5.2.1 *The Silicon Semiconductor*

Silicon is the crystal semiconductor that is the most prominent component in electronic devices. Its outstanding characteristics are: steady electric behaviour, wide abundant, and it is easily grown in furnaces. Some outstanding facts about silicon are:

|                        |               |
|------------------------|---------------|
| Atomic Number          | 14            |
| Electron configuration | $3s^2 3p^2$   |
| Electrons per shell    | 2, 8, 4       |
| Crystal structure      | Diamond cubic |

#### *Silicon versus Gallium Arsenide*

**ABUNDANT.** Silicon is abundant and cheap to process.

**SILICON DIOXIDE** Silicon dioxide can easily be incorporated onto silicon circuits, and such layers are adherent to the underlying Si. GaAs does not form a stable adherent insulating layer.

**HIGH HOLE MOBILITY.** This high mobility allows the fabrication of higher-speed P-channel-FET's (field effect transistors), which are required for CMOS logic. Consequently, they consume less power.

#### 5.2.2 *Convergence Process*

As explained in **Section 4.3**, page 41, before any attempt to perform a band structure computation via the **DFT** formalism, one *must* find out the most suitable values for three parameters, such that the **DSP** signal

is converged. Namely: the number of  $k$ -points ( $nkpt$ ), the value of the energy cutoff ( $ecut$ ), and the number of conduction bands ( $cband$ ).

STEP 1. Convergence on the number of  $k$ -points. To work out the convergence process on  $nkpt$ , the DSP signal was computed for about 15 values of them, with *low* and fixed values of  $ecut$  and  $cband$  (6 Ha and 2 bands, respectively).

18,424  
 $k$ -points

The Figure 6 on page 50 contains the most significant results, and the small inset in it has the two-to-last  $nkpt$  tested values. Because of the small magnitude of  $ecut$  and  $cband$ , the obtained signal resembles more a set of bonded lines than a smooth signal. One can conclude from the figure that, increasing the  $nkpt$  value beyond 18,424  $k$ -points (see the inset) leaves the signal almost unchanged. Therefore the value of 18,424  $k$ -points is taken as the convergence value.

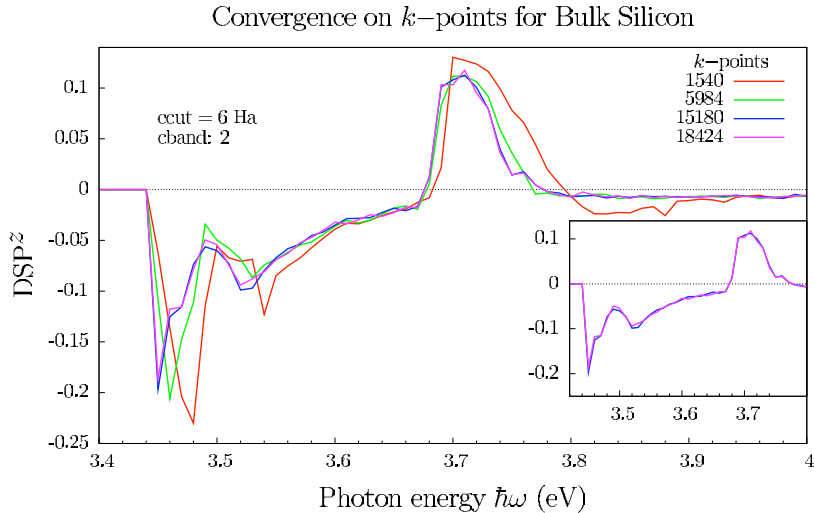


Figure 6: (color online) Convergence of the DSP signal as a function of the number of  $k$ -points for bulk silicon. Used an increasing number of  $k$ -points with *low* and fixed values of energy cutoff ( $ecut$ ) and conduction bands ( $cband$ ). The inset contains only the last two signals, and shows that acceptable convergence is reached at 18,424  $k$ -points.

STEP 2. Convergence on Energy Cutoff. With the converged  $nkpt$  value of STEP 1, and a fixed low value of  $cband$  (2 bands), the DSP response is computed for a set of 10 different energy cutoff values.

30  
Hartrees

The Figure 7 on page 51 shows the most notable DSP responses as a function of the photon energy and the inset in it displays the two highest signals in  $ecut$ . From it, one concludes that a further

increase of `ecut` above 30 Hartrees leaves the `DSP` signal almost unchanged.

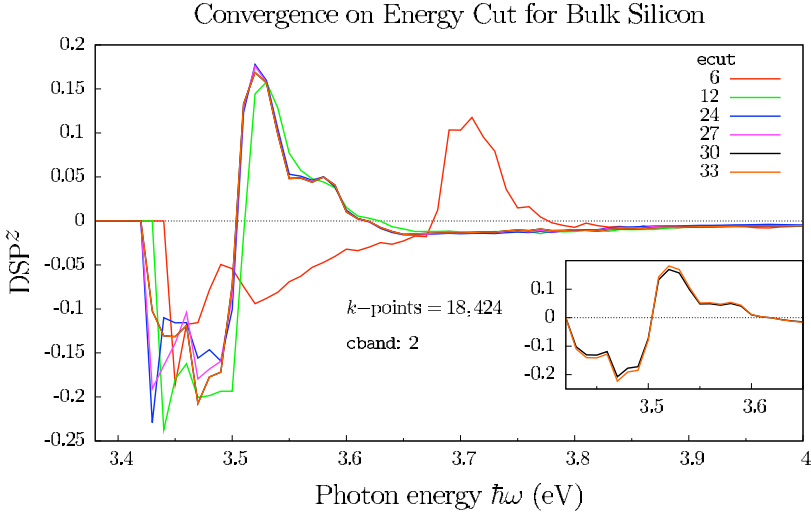


Figure 7: (color online) Convergence of the `DSP` signal as a function of the energy cutoff for bulk silicon. Used increasing values of energy cutoff (`ecut`) with a *low* and fixed value of conduction bands (`cband`) and 18,424  $k$ -points (converged value, see Figure 6 on p. 50). The inset contains only the last two signals, and shows that acceptable convergence is reached at 30 Hartrees.

STEP 3. Convergence on the number of conduction bands. In the last step of the convergence process one takes the converged values of the preceding steps and computes the `DSP` for a number of conduction bands.

The Figure 8 on page 52 shows the most significant `DSP` responses and the inset in it presents the two highest signals in `cband`. From it, one concludes that further increase of `cband` above 8 conduction bands leaves almost unchanged the `DSP` signal.

*In brief*

The `DSP` signal for bulk silicon is well converged for the following set of values: `nkpt`  $\sim$  18 000, `ecut` = 30 Ha, and `cband` = 8 bands.

### 5.2.3 Stress Modulation of DSP

In this section the `DSP` response is computed for different values of volumetric changes, induced by expansive or compressive stresses, as explained in Section 4.4. For this purpose the values of `nkpt`, `ecut`, and

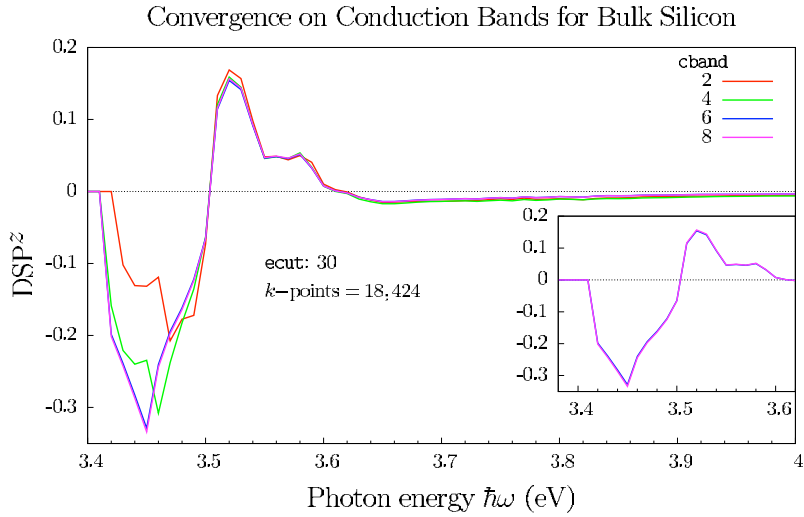


Figure 8: (color online) Convergence of the DSP signal as a function of the number of conduction bands on silicon. Used increasing values of conduction bands (`cband`) with 18,424  $k$ -points and 30 Hartrees of energy cutoff (`ecut`), which are the converged values (see Figure 6 on p. 55 and Figure 7 on p. 51). The inset contains only the last two signals, and shows that excellent convergence is reached at 8 conduction bands.

`cband` adequate for the convergence of the DSP signal were used. The Figure 9 on page 53 displays the obtained results. In it one can realize that, qualitatively,

- Compressive stress shortens and shifts the DSP signal to higher energies.
- Expansive stress augments and shifts the DSP signal to lower energies.
- The overall signal *does* change: the downward peak at compressed states changes polarity and splits in two upward peaks as the bulk silicon undergoes a volumetric expansion from  $-8\%$  to  $+8\%$ .



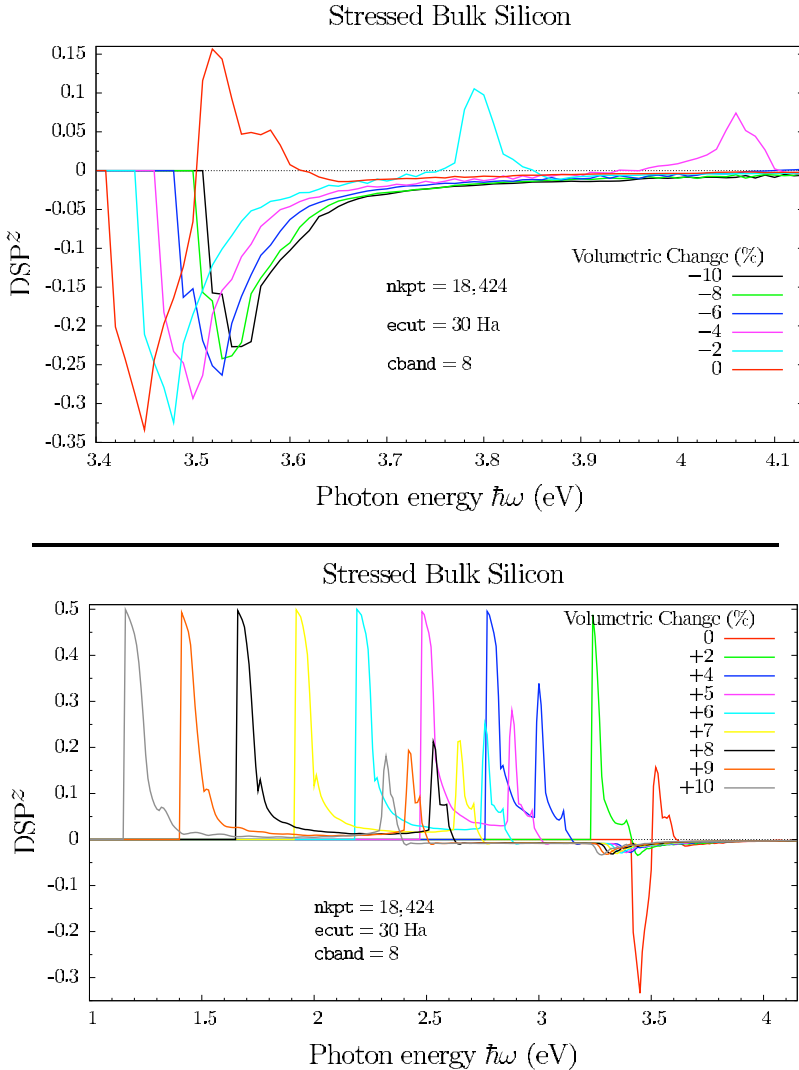


Figure 9: (color online) Stress modulation of the DSP on silicon. Computed with 18,424 k-points, 8 conduction bands (cband), and an energy cutoff (ecut) of 30 Hartrees (values for DSP convergence, see Figure 6, Figure 7, and Figure 8 on pages 50, 51, and 52, respectively). The upper (lower) figure shows the DSP signals for compressive (expansive) stresses. Both figures display that, qualitatively, compressive (expansive) stress effectively modulates the DSP signal on energy operation, and that the overall signal *does* change. Notably, the downward peak at all compressive stresses (all signals in the upper plot, and the unstressed (0%) signal in the lower plot), changes its polarity and splits into two upward peaks as the sample undergoes a volumetric expansion.

## 5.3 EXAMPLE 2. BULK GALLIUM ARSENIDE STUDY

5.3.1 *The Bulk Gallium Semiconductor*

The gallium arsenide (GaAs) is a semiconductor that has a Zinc Blende crystal structure. It is composed by two elements, gallium and arsenic and is mainly used to make semiconductor devices, like electronic circuits, solar cells, diodes, etc.

Gallium is a byproduct of the smelting of other metals, notably aluminum and zinc, and it is rarer than gold. Arsenic is not rare, but it is poisonous.

Electrons per shell 2, 8, 4

Crystal structure Zinc Blende

*GaAs versus Silicon*

GaAs has several characteristics that makes it excel silicon on *some* applications. The most notables are (Ref. [5]):

**DIRECT GAP.** GaAs is a direct gap semiconductor, what makes it most suited for manufacturing *optoelectronic devices*, like detectors devices. Actually, its absorptivity is so high that it requires a cell only a few microns thick to absorb sunlight.

**DRIFT MOBILITY.** GaAs has a better *drift mobility*, allowing it to be used in high speed logic circuit.

**MICROWAVE OPERATION.** GaAs can be operated on microwave frequencies, and silicon not. Therefore GaAs is suited for Gunn and Impatt Diodes, receivers for satellite broadcasting and radars.

**IONIZING RESISTANCE.** Compared with silicon, GaAs has a large resistivity to ionization, which is composed by subatomic particles or waves that are energetic enough to detach (ionize) electrons from atoms or molecules<sup>1</sup>.

5.3.2 *Convergence Process and DSP Modulation*

The gallium arsenide was studied with the same *modus operandi* than the bulk silicon, and here only the results are given. Apart from the computed DSP signals on this thesis, an experimental plot of the DSP

<sup>1</sup> Ionizing ability depends on the energy of the impinging individual particles or waves, and not on their number (refer to the photoelectric effect elsewhere). Examples of ionizing radiation are  $\alpha$  and  $\beta$  radiation, as well as photonic in the short wavelength end (ultraviolet, x-rays, and gamma rays).

dynamics is shown on Figure 13. It was reported by Bhat et al. on Ref. [9]. The figure shows, as they point, *the dynamics of the DSP of electrons after one-photon (closed squares) and two-photon (open circles) excitation*.

Finally, on Figure 15, the modulation of DSP is presented. Notably, the figure only shows the DSP signal till a volumetric expansion of +1.5%, because it was not possible to obtain signals at further expansions. Apparently the implemented scheme of computation (DFT, LDA, *acell* variation, etc) envisions that the band gap of GaAs becomes null for volumetric expansions onward  $\approx 2\%$ .

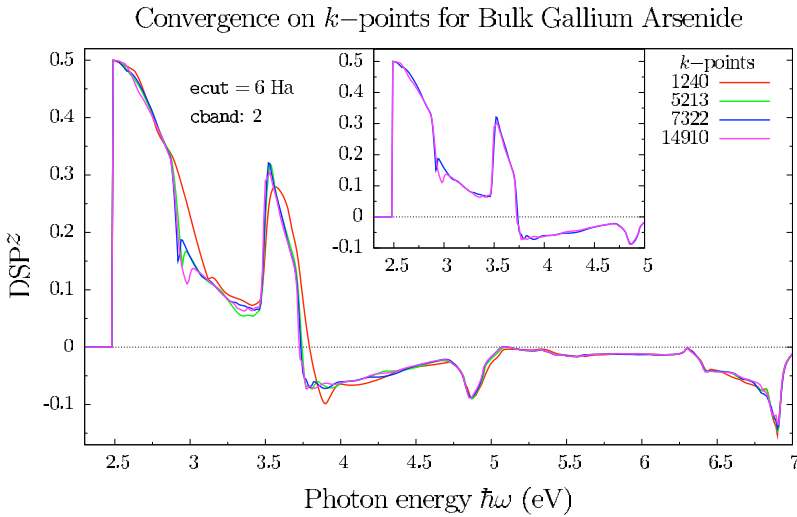


Figure 10: (color online) Convergence of the DSP signal as a function of the number of  $k$ -points with *low* and fixed values of energy cutoff (*ecut*) and conduction bands (*cband*). The inset contains only the two last signals, and shows that acceptable convergence is reached at 14,910  $k$ -points. See the comment on the body text about the window at 3 eV (inset).

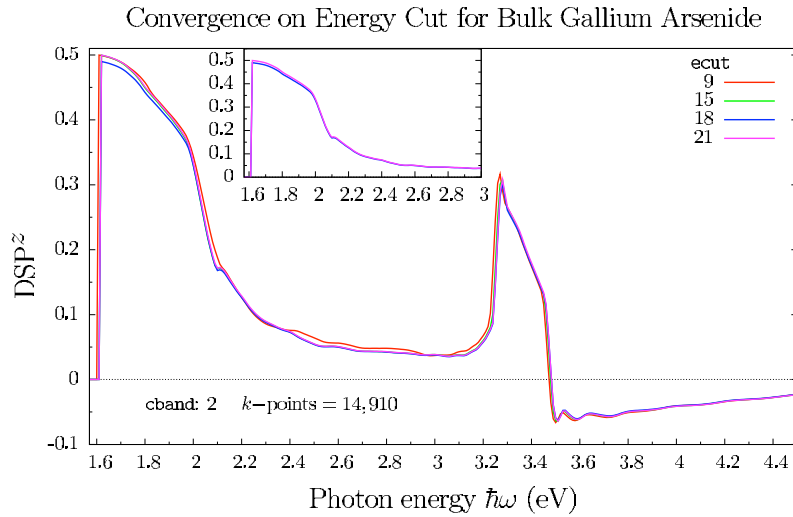


Figure 11: (color online) Convergence of the DSP signal as a function of the energy cutoff on GaAs. Used increasing values of energy cutoff (**ecut**) with a *low* and fixed value of conduction bands (**cband**) and 14,910  $k$ -points (converged value, see Figure 10 on p. 55). The inset contains only the last two signals, and shows that acceptable convergence is reached at 21 Hartrees.

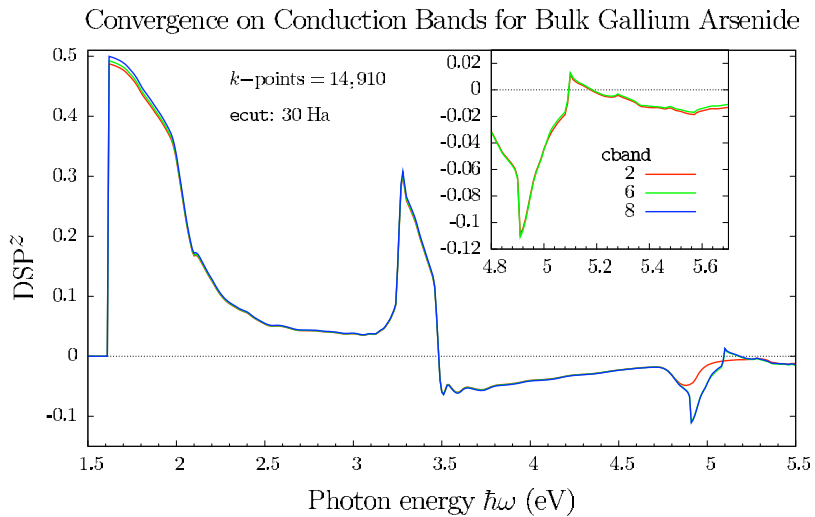


Figure 12: (color online) Convergence of the DSP signal as a function of the number of conduction bands on GaAs. Used increasing numbers of conduction bands (**cband**) with 14,910  $k$ -points and 21 Hartrees of energy cutoff (**ecut**), which are the converged values (see Figure 10 on p. 55 and Figure 11 on p. 56). The inset contains only the last two signals, and shows that excellent convergence is reached at 8 conduction bands.

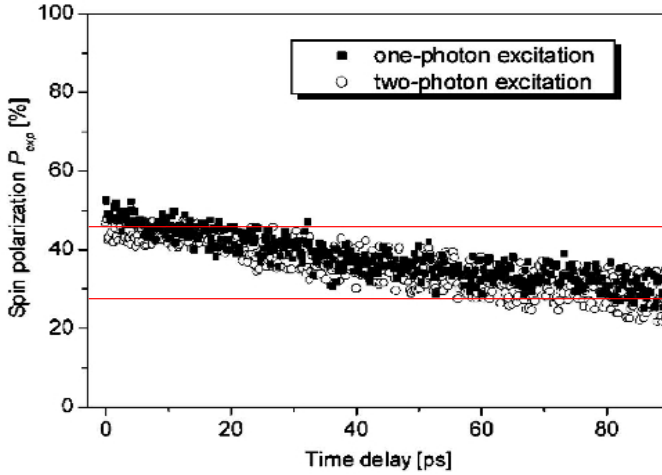


Figure 13: Experimental measurement of the DSP on bulk GaAs, as reported by Bhat et al. on Ref. [9]. The figure shows, as they point, the dynamics of the DSP of electrons after one-photon (closed squares) and two-photon (open circles) excitation. Notice that the DSP signal decays from 48% to 28% in about 90 seconds. Considering the decay remains linear, the DSP signal would fall to zero in about  $225 \times 10^{-12}$  seconds. Compare with the computed signal in this thesis, Figure 15.

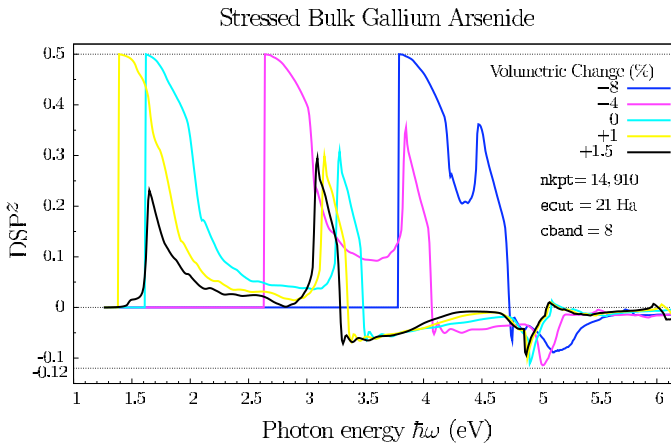


Figure 14: (color online) Stress modulation of DSP on GaAs. Computed with 14,910  $k$ -points, 8 conduction bands ( $cband$ ), and an energy cutoff ( $ecut$ ) of 21 Hartrees (values of convergence, see Figure 10, Figure 11, and Figure 12). Qualitatively, the DSP signal is compacted (enlarged) and shifted to higher (lower) energies by compressive (expansive) stresses. Moreover, stress does not change significantly the DSP peak values. Expansive stress causing volumetric changes greater than 1.5% could not be computed, see the body text for an explanation.



## SUMMARY AND CONCLUSIONS

*All endeavor calls for the ability to tramp the last mile,  
shape the last plan, endure the last hours toil.  
The fight to the finish spirit is the one characteristic  
we must possess if we are to face the future as finishers.*

—Henry David Thoreau  
American Philosopher and Activist

## 6.1 SUMMARY

The thesis work presented here is part of the research I performed under the supervision of Dr. Bernardo Mendoza during my Master in Science studies at Centro de Investigaciones en Óptica, A.C. (León, México). Its main objectives are (1) to investigate the well known fact that the optical electron spin-injection on bulk semiconductors is affected by the application of stresses, and (2) to explore the possibility of modulate such phenomenon by either compressive or expansive stresses. For that matter, a simple and effective method to compute the spin injection as a function of stress (or a related quantity) was proposed, considering both compressive and expansive stresses.

The scheme is to consider that the applied stress induces a hypothetical variation of the bulk sample and consider that variation as the independent variable. Then the whole sample volume can be thought as a stack of primitive unit cells rooted at the Bravais lattice points. The primitive unit cell depends on the primitive translational vectors (`rprimd`) through Equation 4.7 and Equation 4.8. In turn, `rprimd` depends on the `ABINIT`'s `sCAle CELL` parameter (`acell`) and the primitive unit vectors (`rprim`) via Equation 4.9. Therefore, the volumetric variation of the sample due to the applied stress can effectively be indicated through a variation in `acell`.

After that, the spin and position matrix elements required to evaluate the `DSP` expressions (Equations 4.2 on page 37) are computed for each variation of the `acell` parameter, employing a band structure calculation within the `DFT` with `LDA` pseudo-potentials.

## 6.2 CONCLUSIONS

## IN GENERAL

- Optical spin injection can be optimized, in magnitude and energy-operation, by applying either expansive or compressive stresses.
- Material properties in crystalline semiconductors (like the band structure, the linear and nonlinear susceptibilities, the DSP, etc.) can be calculated for strained samples by computing such properties with the **ABINIT** software and varying the program's **acell** parameter to simulate an hypothetical volumetric change due to the stress.

## FOR BULK SILICON (Left plot of Figure 15)

- It is more spin-polarizable at expansive stress (DSP peak  $\sim 50\%$ ) than at compressive stress (DSP peak  $\sim -20\%$ ) or unstressed state (DSP peak  $\sim -30\%$ ).

## FOR BULK GALLIUM ARSENIDE (Right plot of Figure 15)

- It is roughly equally spin-polarizable at compressive, expansive, or unstressed states (DSP peak  $\sim 50\%$ ), but the application of expansive stress can shift the range of operation to a more suitable energy (in the experimental sense).

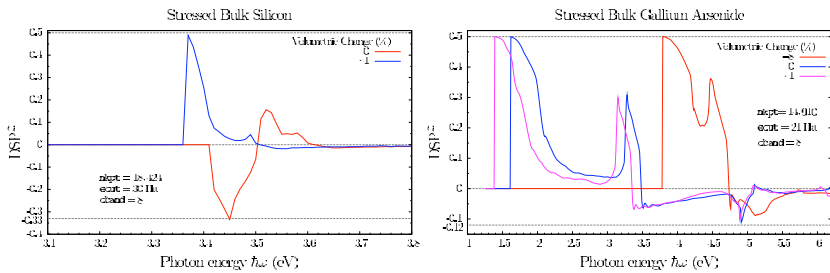


Figure 15: (color online) Some particular results of the DSP modulation by applied stress. The complete set appear at full scale on pages 53 and 57 (Figure 9 and Figure 14)



Part IV

APPENDIX



## A.1 “FREE SOFTWARE, FREE SOCIETY”



*Free software is a matter of the users' freedom to run, copy, distribute, study, change and improve the software.*

— Richard M. Stallman [35]

*The free software movement was started in 1983 by computer scientist Richard M. Stallman, when he launched a project called GNU ([www.gnu.org](http://www.gnu.org)), which stands for “GNU is Not UNIX”, to provide a replacement for the UNIX operating system — a replacement that would respect the freedoms of those using it. Then in 1985, Stallman started the Free Software Foundation ([www.fsf.org](http://www.fsf.org)), a nonprofit organization with the mission of advocating and educating on behalf of computer users around the world [...]*

*To use free software is to make a political and ethical choice asserting the right to learn, and share what we learn with others. Free software has become the foundation of a learning society where we share our knowledge in a way that others can build upon and enjoy.<sup>1</sup>*

...

The computational tools employed at the Optics Surface Group

<http://aida.cio.mx/>

at Centro de Investigaciones en Óptica, A.C. use almost exclusively free(ware) software, being the only exception the use of the Apple's OSX. Apart of the advantage of being costless, free(ware) software gives us the opportunity to adapt and develop our own tools, like the TINIBA shells, detailed in [Section A.2](#).

For instance, the present thesis employed the [ABINIT](#) software to compute the band structure calculations, together with a set of FORTRAN modules. Both of them are controlled by a set of BASH scripts ([TINIBA](#)). The figures were produced with [GNUPLOT](#) and [XFIG](#), and the thesis document was typeset with the [classicthesis](#) style. The edition process was done on *the* [EMACS](#) editor.

<sup>1</sup> Taken from <http://www.fsf.org/about/what-is-free-software>.

## A.2 TINIBA: A SET OF BASH SCRIPTS

*We have seen that computer programming is an art,  
because it applies accumulated knowledge to the world,  
because it requires skill and ingenuity, and especially  
because it produces objects of beauty.*

— Donald E. Knuth [36]

**TINIBA** is a computer software that some members of the Surface Optics Group at **CIO** have developed. Its purpose is to perform parallel computations of semiconductor properties, like the electronic structure and the linear and non-linear responses in surface and bulk semiconductors. **TINIBA** is composed by a number of modules written in **BASH**, the standard shell program (command interpreter) of the GNU/Linux operative system, i.e. **TINIBA** is not a compiled program, but one that is interpreted line-by-line.

Interpreted programs have the advantage that they are easy to develop and maintain and that they are slow to perform numerical and string computations. Nevertheless **TINIBA** shells delegate all numerical computations to FORTRAN subroutines that the group has developed in collaboration with **Nastos et al.**, authors of Ref. [1].

Therefore, **TINIBA** shells have the best of two worlds: speed and facility for maintenance and development. In **Figure 16** a simplified **TINIBA**'s flow diagram is displayed, and in **Section A.2.1** a verbose description of it is given.

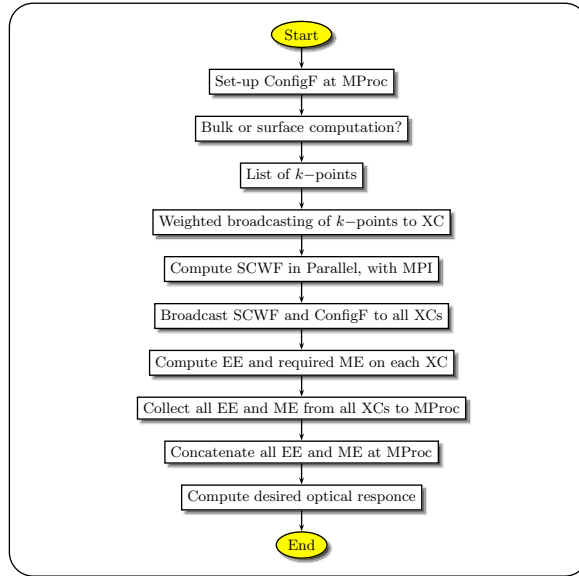
A.2.1 *The TINIBA Modules*

Next the main steps of a standard computation are described. The names in square brackets and typewriter font refer to the name of the bash modules that perform the action.

- A. Set up the configuration-file according to the physical properties of the semiconductor (`setUpAbinit_<foo>.in`), and give the coordinates of the location of each atom in the unit cell [`<foo>.xyz`].
- B. Generate a list of k-points [`rklist.sh`].
- C. Perform a *weighted* distribution of the k-points generated on **item B** over all execution cores. The weight is done according to the speed of each processor, for example, <sup>2</sup>. The objective is that each execution core works out a subset of the k-points [`arrangeMachines.pl`].

---

<sup>2</sup> Roughly, 1 Quad = 2 Itanium = 4 Xeon



**Nomenclature (in order of appearance)**

|         |   |
|---------|---|
| ConfigF | CONFIGURATION Files, according to physical properties.      |
| MProc   | Master PROCessor  |
| XC      | eXecution Core  |
| SCWF    | Self Consistent Wave Function                               |
| MPI     | Message Passing Interface standard for parallel computation |
| EE      | Eigen-Energies  |
| ME      | Matrix Elements   |

Figure 16: TINIBA. Home-made Bash-scripts to compute optical responses in semiconductors.

- D. Broadcast of the configuration-files ([item A](#)) and the subset of the list of  $k$ -points ([item c](#)) [`copySCF2nodes.sh`].
- E. In a single processor, presumably on the master, perform a self-consistent computation of the wave-function [`runSCFxeon.sh`, `runSCFitan.sh`, or `runSCFquad.sh`, depending on the architecture of the selected processors, Xeon, Itanium, or Quad]. The self-consistent files are then broadcasted to all the processors [`copySCF2nodes.sh`].
- F. Compute the eigenenergies and momentum matrix elements on each execution core<sup>3</sup>. The output files of each execution core correspond to the result of a subset of the total number of  $k$ -points [`runBulk.sh`].

<sup>3</sup> Xeon, Itanium, and Quad processors have 2, 2, and 8 execution cores each one, respectively.

- G. The output files of [item F](#) are copied to the master processor and concatenated (linked together in series) in the correct order, according to the list of k-points [concatena.pl].
- H. Optionally, an optical response might be calculated. For example, the first and second order susceptibilities, the spin carrier injection, etc. [response.sh].

## A.3 MEDUSA: THE COMPUTING CLUSTER

The Optics Surface Group (<http://aida.cio.mx/>) at Centro de Investigaciones en Óptica, A.C. owns a computing cluster called MEDUSA. It is composed of several Intel processors of three kinds: Xeon, Itanium, and Quad Core. Each processor has its own hard disk and RAM memory (see Figure 18).

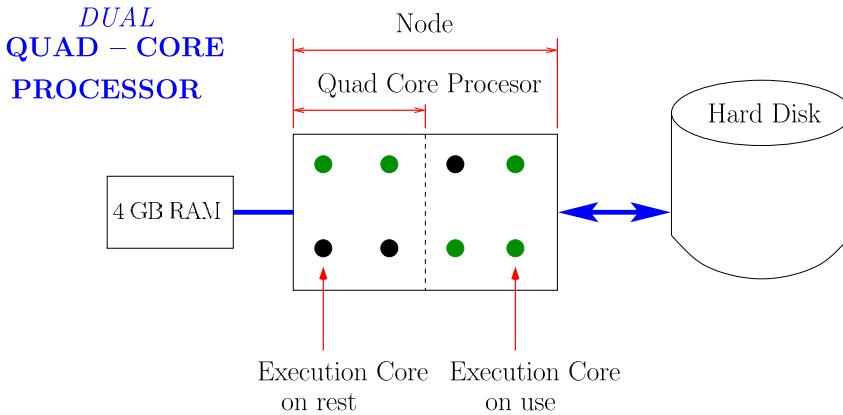
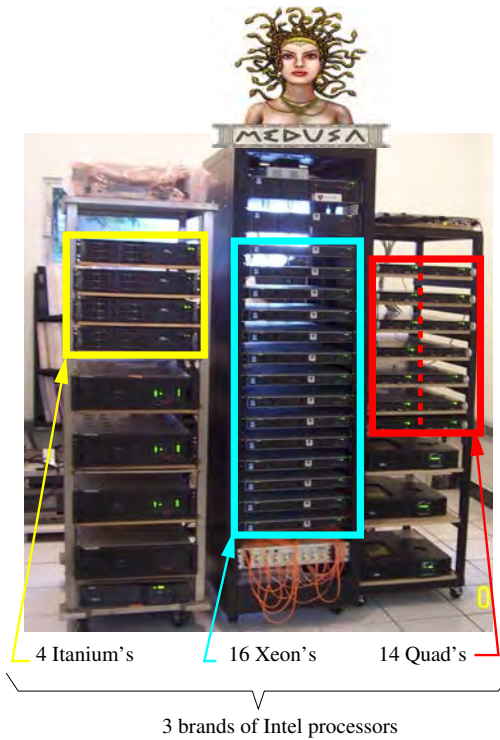


Figure 17: Schematic representation of a Medusa's Quad processor.

Each processor has a different number of execution cores. For instance, the Dual Quad-Core Processors (see Figure 17) have two processors, each of them with four execution cores, summing then eight execution cores 'per Quad'. The Xeon and Itanium processors are 'single processors' with two execution cores. Considering these three brands, Medusa has a total of 152 execution cores (see Figure 18 for a breakdown of facts).



**The cluster**

- 34 computers (nodes)
- per Quad: 2 nodes, per node: 4-cores
- per Itanium: 1 node, per node 2-core
- per Xeon: 1 node, per node 2-core

- 8 Itanium cores
- 32 Xeon cores
- 112 Quad cores

**Round numbers:**

- 152 execution cores
- 170 GB of RAM
- 5,720 GB of HDisk

**Software tools:**

- GNU/Linux CentOS
- MPich & openMP
- LAPACK & ScaLAPACK
- Fortran, Bash, Perl, Python
- Abitin, **Tiniba (home-made)**

Edited with XFIG  
a 'free' drawing tool

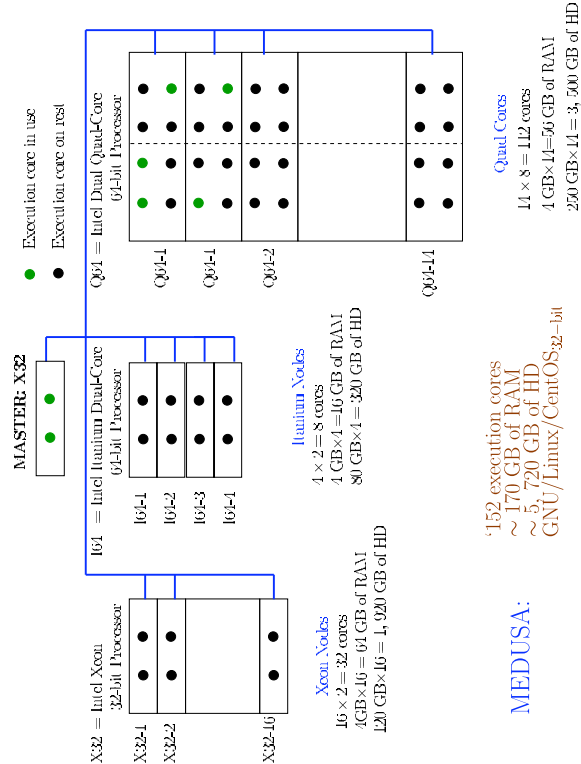


Figure 18: Medusa: The group's cluster computer.



## A.4 PERFORMANCE OF THE COPY AND ABINIS PROCESSES

The computation of the self consistent wave-function and the band structure (eigen-energies for each  $k$ -point) require much less time to be completed than the the computation of the matrix elements for the position, momentum, and spin. Therefore, these computations are done in parallel, with some selected (by hand) set of cores performing a part of the computation.

**TINIBA** calculates the matrix elements in such a manner that each 'execution core' has its own self-consistent wave-function (SCWF) to do its job, i.e. it requires to replicate this function as many times as execution cores we decide to use.

For typical surface calculations, like surface responses, the SCWF's size can be as large as 2 Giga Bytes, therefore, the replication needs significant machine resources. For each replica: split the function into manipulable small files, transport the small files thoughtout the buss, concatenate all the small files to recover the original. Then naturally a question arose: Could we cut down resources if each core shares a single SCWF per node?

To address this question, a typical surface computation of matrix elements was done, employing a SCWF of 1.2 GB on a single QUAD processor (see [Figure 17](#) on page 67). As commented above, such kind of processor possesses 8 execution cores. Two scenarios were studied:

**SINGLE COPY CASE.** (standard procedure) All the selected execution cores share a single SCWF.

**MULTI COPY CASE.** All the selected execution cores possess their own SCWF.

Then two experiments were performed, a Copy Experiment and a Matrix Elements Computation Experiment. Each of them starting with only one execution core, both experiments were carried out 8 times for each case, increasing in one the number of employed execution cores each time. The results appear on page 70, [Table 1](#) and [Figure 19](#).

The conclusions from these experiments are:

**COPY EXPERIMENT.** It is faster to broadcast single copies than multi-copies, which is natural. The importance of this experiment relies on the quantification of the time differences. The biggest difference is at 8 execution cores (with 8  $k$ -points), with a difference of about 15 minutes.

**MATRIX ELEMENTS EXPERIMENT.** It is faster to compute the matrix elements with a multi-copy scheme than with the single-copy scheme. The time difference is about 410 min (6.8 hours).

| Cores &<br>k-points | Copy Experiment |            | Matrix Elements Experiment |            |
|---------------------|-----------------|------------|----------------------------|------------|
|                     | Single-Copy     | Multi-Copy | Single-Copy                | Multi-Copy |
| 1                   | 3.8             | 5.3        | 225.4                      | 143.3      |
| 2                   | 3.7             | 5.5        | 153.3                      | 152.6      |
| 3                   | 3.7             | 7.9        | 448.0                      | 452.2      |
| 4                   | 3.7             | 9.8        | 515.1                      | 508.4      |
| 5                   | 3.7             | 12.3       | 870.8                      | 687.7      |
| 6                   | 5.9             | 13.8       | 1367.9                     | 947.0      |
| 7                   | 5.3             | 17.3       | 1659.2                     | 1383.1     |
| 8                   | 6.0             | 20.0       | 2310.4                     | 1900.1     |

Table 1: Single- and Multi-Copy Benchmarking. Required times, in minutes, to complete the copy and matrix elements experiments. The number of execution cores is equal to the number of sampled k-points.

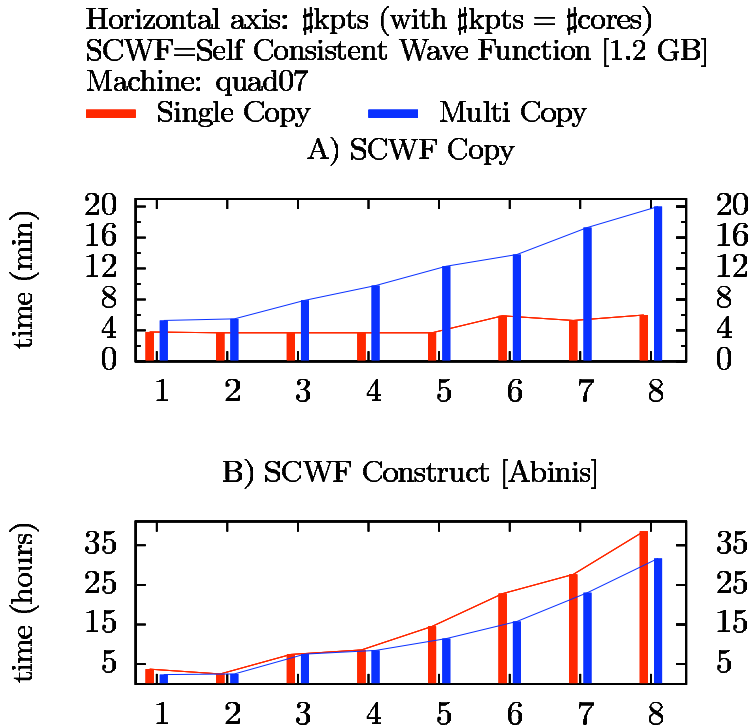


Figure 19: Performance of the Copy and Abinis Processes.


The results of this thesis were presented on October 21, 2008 at the "LI Congreso Nacional de Física" (60<sup>th</sup> National Congress of Physics) held at Zacatecas, México. The poster session was the 2MA02.

### Software Development for Numerical Calculation of Optical Spin Injection on Stressed Bulk Semiconductors

Cuauhtémoc Salazar<sup>1</sup>, J.L. Cabellos<sup>2</sup>, and Bernardo S. Mendoza<sup>3</sup>

<sup>1</sup>tsalazar@icmex.izt.ac.mx, <sup>2</sup>lcabello@icmex.izt.ac.mx, <sup>3</sup>bsmendoza@icmex.izt.ac.mx

Centro de Investigaciones en Óptica A.C.  
León, MEXICO



GNU stands for "Gnu's Not Unix". It is a free software project that provides a complete operating system, including a kernel, shell, utilities, and libraries. It is designed to be a free alternative to Unix.

#### Introduction

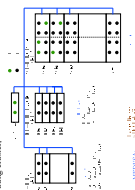
- This work lies in the Semiconductor Spintronics field. A broad description of it can be found in reference [1].
- Spintronics is a new branch of physics that focuses on the spin of electrons as a new generation of microelectronic based not on the electron's charge, but on the quantum intrinsic angular momentum property called spin. Electrons, holes, neutrons, and photons are the particles that carry spin.
- In practice, spintronic research involves electronics, magnetism, optics, and materials science.
- Advantages of spins over charges are easy manipulation, low energy consumption, less power requirements, and many binary logic.
- The long time goal is to produce spintronic devices that integrate electronics, optoelectronic, and magneto-electronic functionalities.
- Spintronic devices are made by the Giant Magnetoresistance (GMR) effect, the Tunneling Magnetoresistance (TMR) effect, the Spin-Transfer Torque (STT) effect, the Spin-Orbit Torque (SOT) effect, and in any high conductivity magnetic sensor.
- Other fields like Spin-Transistor (Datta and Das, 1990), All-Metal Spin-Transistor (Mark Johnson, 1994), Spin-Polarized Solar Cells,
- Spintronic quantum-gates for quantum computing.
- Early evidences of spin effects also from the observation of the anomalous Hall effect (AHE) in ferromagnetic metals (Zeman effect (1921), the Stern-Gerlach experiment (1922), and the magnetization of ferromagnets.
- But, since those observations couldn't be explained with theory required *relativistic corrections* that included mass, time, and length variations, as well as magnetic effects.
- In 1928 Wolfgang Pauli proposed a new degree of freedom (intrinsic spin) to explain the anomalous Hall effect with a Pauli solved the inconsistencies between the observed magnetic systems and the emerging quantum theory (intrinsic spin) as an intrinsic electron spin. In 1927 Pauli completed its spin theory with the addition of the Pauli matrices as a basis of spin operators of the Pauli matrices as a basis of spin operators.
- In 1928 the British Pauli Dirac provided a relativistic quantum mechanical wave equation that was consistent with the experimental results of the Stern-Gerlach experiment. Dirac's description is a formal formulation of quantum mechanics, and Pauli's formalism is a limiting case when the electron's speed is small compared with that of light.

#### Optical Spin Injection

- Spin injection is the process of injecting a net spin of conduction electrons into a semiconductor of circularly polarized light. Other schemes of spin injection exist, like electric or transport injection from a ferromagnet.
- In addition to electrons, neutrons, and photons also interact with spin.
- When a photon is absorbed it transfers its linear momentum to the medium. If the photon is circularly polarized, it transfers its angular momentum, creating a torque to the medium and optical orientation effects.

#### Computational Details

The expressions were evaluated with MATHEMATICA, the group's computing system.

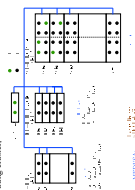


In this work we aimed to explore the DSP responses to the spin injection rate, given by the following expression (6) and (7) for suitable points where DSP is maximized.

$$\text{DSP} = \frac{S^x}{\gamma} \quad (6)$$

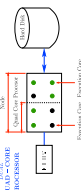
where  $\gamma$  is the carrier injection rate, given by

$$\gamma = e^{\frac{1}{2} \ln \left( \frac{1 + \beta \cos \theta}{1 - \beta \cos \theta} \right)} \quad (7)$$



The expressions were evaluated with MATHEMATICA, the group's computing system.

composed by 132 execution errors with the operative system GNU/Linux (CentOS Distribution)



To implement the DFT band structure calculation we used our house-made FORTRAN libraries; both of them manipulated with MATLAB.

**Personal Contribution:** Modification of the existent FORTRAN code to calculate the DSP for a any amount of compression expansion or spin.

#### Conclusions

- Optical spin injection can be optimized, in magnitude and energy operation, by applying expansion strain.
- Optical spin injection is more efficient at a strain state (~20%) than at compressive strain (~20%) or unstained state (~20%).
- Bulk GaAs is roughly equally polarizable at compression and expansion, but the strain-induced application of expansion strain can shift the range of application to a more suitable energy.

#### Future Work

- Include non-isotropic compression/expansions.
- Complete spin transport and spin relaxation calculation.

#### References

- [1] F. Heide, J. Rinow, M. Szymanski-Majewski, Bernardo S. Mendoza, and J. L. Cabellos, "Numerical calculation of optical spin injection," *Phys. Rev. B*, vol. 76, p. 2007, 2007.
- [2] Zinic, Fabian, and Das-Sarma, "Spintronics: Fundamentals and applications," *Rev. Mod. Phys.*, vol. 78, p. 2004, 2006.

Figure 20: Poster at the National Congress of Physics, Zacatecas, México.



## BIBLIOGRAPHY

---

- [1] F. Nastos, J. Rioux, M. Strimas-Mackey, Bernardo S. Mendoza, and J. E. Sipe. Full band structure  $l$ da and  $\mathbf{k} \cdot \mathbf{p}$  calculations of optical spin-injection. *Phys.Rev. B*, 76, 2007. (Cited on pages xi, 23, 39, 41, and 64.)
- [2] B.S. Mendoza, F. Nastos, N. Arzate, and J.E. Sipe. Layer-by-layer analysis of the linear optical response of clean and hydrogenated Si(100) surfaces. *Phys.Rev. B*, 74:075318, 2006. (Cited on pages xi and 39.)
- [3] Erich Fromm. *The Art of Being*. Continuum, 1992. Edited by Rainer Funk. (Cited on pages xiii and xv.)
- [4] Bernardo Mendoza Santoyo, José Luis Cabellos Quiroz, and Tonatiuh Rangel Gordillo. *TINIBA, Programs for the parallel computation of optical responses on semiconductors on a computer cluster*. Centro de Investigaciones en Óptica, A.C. (Cited on page xxii.)
- [5] Allingworth and Cullerne. *The Penguin Dictionary of Physics*. Longman, 3 edition, 2000. (Cited on pages 4 and 54.)
- [6] S.A. Wolf, A.Y. Chtchelkanova, and D.M. Treger. Spintronics – a retrospective and perspective. *IBM Journal of Research and Development*, 50(1), January 2006. (Cited on page 5.)
- [7] Sankar Das Sarma. Spintronics. *American Scientist*, 89:516–523, November-December 2001. (Cited on pages 5 and 11.)
- [8] A. Najmaie, R.D.R. Bhat, and J.E. Sipe. All-optical injection and control of spin and electrical currents in quantum wells. *Physical Review B*, 68, 2003. (Cited on pages 5 and 32.)
- [9] R.D.R. Bhat, P. Nemeč, Y. Kerachian, H. M. vanDriel, J. E. Sipe, and Arthur L. Smirl. Two-photon spin injection in semiconductors. *Phys.Rev.B*, 2005. (Cited on pages 5, 55, and 57.)
- [10] Igor Žutić, Jaroslav Fabian, and S. Das Sarma. Spintronics: Fundamentals and applications. *Rev.Mod.Phys.*, 76, 2004. (Cited on pages 5, 6, 8, 9, and 10.)
- [11] Ammon Yariv and Pochi Yeh. *Photonics, Optical Electronics in Modern Communications*. Oxford University Press, 2007. (Cited on page 6.)

- [12] Mathias Duckheim and Daniel Loss. Electric-dipole-induced spin resonance in disordered semiconductors. *Nature Physics* 2, (), 2:195 – 199, 2006. doi:10.1038/nphys238. (Cited on page 7.)
- [13] Vitaly N. Golovach, Massoud Borhani, and Daniel Loss. Electric dipole induced spin resonance in quantum dots. *Physical Review B*, 74:165319, 2006. URL <http://www.citebase.org/abstract?id=oai:arXiv.org:cond-mat/0601674>. (Cited on page 7.)
- [14] D.D. Awschalom, D. Loss, and N. Samarth, editors. *Semiconductor Spintronics and Quantum Computation*. Springer, 2002. (Cited on pages 8 and 74.)
- [15] S. Datta and B. Das. Electronic analog of the electro-optic modulator. *Appl.Phys.Lett.*, 56, 1990. (Cited on page 10.)
- [16] Mark Johnson. Bipolar spin switch. *Science*, 260, 1993. (Cited on pages 10 and 11.)
- [17] David P. Di Vincenzo. Quantum computing. In Awschalom et al. [14], chapter chapter pending, page 222. (Cited on page 11.)
- [18] B.E. Kane. A silicon-based nuclear spin quantum computer. *Nature*, 393:1331, 1998. (Cited on page 12.)
- [19] Walther Gerlach and Otto Stern. Das magnetische moment des silberatoms. *Zeitschrift fur Physik*, 9:353–355, 1922. (Cited on page 15.)
- [20] L. de la Peña. *Introducción a la Mecánica Cuántica*. FCE-UNAM, 3 edition, 2006. (Cited on pages 16 and 17.)
- [21] C. Cohen-Tannoudji, B.Diu, and F. Laloë. *Quantum Mechanics*, volume 2. John Wiley and Sons, 1977. 2005 reprint. (Cited on pages 17 and 18.)
- [22] Nathan Argaman. Density functional theory: An introduction. *Am.J.Phys*, 2000. (Cited on pages 23 and 39.)
- [23] R.O. Jones and O. Gunnarsson. The density functional theory, its applications and prospects. *Rev.Mod.Phys.*, 61(3):689, July 1989. (Cited on pages 23 and 39.)
- [24] J. Kevorkian and J. D. Cole. *Multiple Scale and Singular Perturbation Methods*. Springer-Verlag, 1996. (Cited on page 25.)
- [25] Melvin Lax. *Symmetry Principles in Solid State and Molecular Physics*. Dover Publications, 2001. Chap. 10. (Cited on page 32.)

- [26] P. Hohenberg and W. Kohn. Inhomogeneous electron gas. *Phys. Rev.*, 136(3B):B864–B871, Nov 1964. doi: 10.1103/PhysRev.136.B864. (Cited on page 38.)
- [27] W. Kohn and L. J. Sham. Self-consistent equations including exchange and correlation effects. *Phys. Rev.*, 140(4A):A1133–A1138, Nov 1965. doi: 10.1103/PhysRev.140.A1133. (Cited on page 38.)
- [28] S.M. Blinder. Basic concepts of self-consistent-field theory. *American Journal of Physics*, 33(6), June 1965. (Cited on pages 38 and 39.)
- [29] M. C. Payne, M. P. Teter, D. C. Allan, T. A. Arias, and J. D. Joannopoulos. Iterative minimization techniques for ab initio total-energy calculations: molecular dynamics and conjugate gradients. *Rev. Mod. Phys.*, 64(4):1045–1097, Oct 1992. doi: 10.1103/RevModPhys.64.1045. (Cited on pages 38 and 39.)
- [30] A. Mujica, Angel Rubio, A. Mu noz, and R.J. needs. High-pressure phases of group-iv, iii-v, and ii-vi compounds. *Rev.Mod.Phys.*, 75 (3):863–912, July 2003. (Cited on pages 39, 42, and 43.)
- [31] R. M. Martin. *Electronic Structure. Basic Theory and Practical Methods*. Cambridge University Press, 1 edition, 2008. (Cited on page 39.)
- [32] X. Gonze, J.-M. Beuken, R. Caracas, F. Detraux, M. Fuchs, G. M. Rignanese, L. Sindic, M. Verstraete, G. Zerah, F. Jollet, M. Torrent, A. Roy, M. Mikami, Ph. Ghosez, J.-Y. Raty, and D. C. Allan. First-principles computation of material properties: the ABINIT software project. *Comput. Mater. Sci.*, 25(478), 2002. (Cited on page 39.)
- [33] Stefan J. Turneure and Y. M. Gupta. Inelastic deformation and phase transformation of shock compressed silicon single crystals. *Appl.Phys.Lett.*, 91, 2007. DOI: 10.1063/1.2814067. (Cited on page 44.)
- [34] N. W. Ashcroft and N. D. Mermin. *Solid State Physics*. Brooks Cole, 1976. (Cited on page 44.)
- [35] Richard M. Stallman. *Free Software, Free Society: Selected Essays of Richard M. Stallman*. GNU Press. Free Software Foundation [www.fsf.org](http://www.fsf.org), 2002. [www.gnupress.org](http://www.gnupress.org). (Cited on pages 63 and 79.)
- [36] Donald E. Knuth. Computer Programming as an Art. *Communications of the ACM*, 17(12):667–673, December 1974. (Cited on page 64.)
- [37] Robert Bringhurst. *The Elements of Typographic Style*. Version 2.5. Hartley & Marks, Publishers, Point Roberts, WA, USA, 2002. (Cited on page 79.)





## INDEX

---

- Anvil cell, [43](#)
- Atomic unit system, [42](#)
  
- Bohr Magneton, [6](#), [17](#)
- Bravais Lattice, [44](#)
- Brillouin zone, [40](#)
  
- Cluster, computing, Medusa, [67](#)
- Coherent excitations, [24](#), [43](#)
- Convergence analysis, [41](#)
- Current, electric, [3](#)
  
- DAC, diamond anvil cell, [43](#)
- Density-functional theory, [38](#)
- Devices
  - Datta-Das Transistor, [10](#)
  - FET, [10](#)
  - GMR sandwich, [9](#)
  - LED, [10](#)
  - quantum computer, [11](#)
  - solar cells, [11](#)
- DFT, [23](#)
- Domains, ferromagnetic, [5](#)
- DSP, [23](#)
  - modulation on GaAs, [54](#)
  - modulation on silicon, [51](#)
  
- Electrical
  - Spin-Polarization, [6](#)
- Equation
  - Schrödinger, [16](#)
  - Kohn-Sham, [38](#)
  - Dirac, [17](#)
  - Klein-Gordon, [16](#)
  - of motion, [23](#)
    - multi-scale solution, [25](#)
    - perturbative solution, [28](#)
  - Pauli, [17](#)
  
- Free software, [63](#)
  
- GaAs study, [54](#)
- GMR device, [9](#)
  
- interaction representation, [30](#)
  
- JDOS integrals, [40](#)
  
- Kohn-Sham equations, [38](#)
  
- Matrix Elements
  - position, [37](#)
  - spin, [37](#)
- Matrix elements
  - interband, [25](#)
  - intragand, [25](#)
  
- Nanotechnology, [3](#)
  
- Optical
  - frequencies, [37](#)
- Optical Spin-Polarization, [6](#)
- Optoelectronics, [3](#)
  
- Pauli
  - equation, [18](#)
  - postulates, [18](#)
- Pauli's postulates, [17](#)
- Polarization
  - circular, [6](#)
- Pseudo-tensor, [33](#), [35](#)
  
- Quantization, space, [4](#)
- Quantum
  - bits, [11](#)
  - computer
    - requirements, [11](#)
  - information
    - requirements, [11](#)
- Qubits, [11](#)
  
- Resonant
  - Spin-Polarization, [6](#)

- Schrödinger equation, 16
- Self-consistency, 38
- Silicon
  - convergence process, 50
  - DSP modulation, 51
- Silicon study, 49
- Spin, 3
  - decoherence, 8
  - dephasing time, 8
  - devices, 9
    - FET, 10
  - ensemble relaxation, 8
  - evidences, 15
  - influence, 4
  - injection rate, 23
  - LED, 10
  - matrix elements, 37
  - measurement, 7
  - polarization, 6
  - relaxation, 8
  - relaxation time, 8
- Spin-Polarization
  - Electrical, 6
  - Optical, 6
  - Resonant, 6
- Spintronic, 11
  - devices, 9
    - Datta-Das Transistor, 10
    - GMR, 9
    - LED, 10
  - quantum computer, 11
  - solar cell, 11
- Spintronics, 5
- Stern-Gerlach Experiment, 15
  
- Tetrahedral method, 41
- Tiniba, 64
  - performance, 69

## COLOPHON

Except by the use of the OSX operative system, all the computational tasks performed in this thesis employed solely *Free Software*<sup>1</sup>. This includes the typesetting (L<sup>A</sup>T<sub>E</sub>X with CLASSIC<sub>THE</sub>ISIS style<sup>2</sup>), the figures (GNUPLOT and XFIG), the computations (BASH interpreter, FORTRAN compilers, and ABINIT software) and the cluster's operative system (CENTOS). The edition was done on *the* EMACS editor<sup>3</sup>.

Cuauhtémoc

December, 2008.

Léon, MÉXICO.

*Final Version* as of February 13, 2009 at 18:03.

---

<sup>1</sup> See *Free Software, Free Society: Selected Essays of Richard M. Stallman*, Ref. [35].

<sup>2</sup> By André Miede, <http://www.miede.de>, who states that CLASSIC<sub>THE</sub>ISIS style “was typeset with L<sup>A</sup>T<sub>E</sub>X<sub>2 $\epsilon$</sub>  using Hermann Zapf's *Palatino* and *Euler* type faces (Type 1 PostScript fonts *URW Palladio L* and *FPL* were used). The listings are typeset in *Bera Mono*, originally developed by Bitstream, Inc. as “Bitstream Vera”. (Type 1 PostScript fonts were made available by Malte Rosenau and Ulrich Dirr.)

The typographic style was inspired by *Bringhurst's* genius as presented in *The Elements of Typographic Style* [37]. It is available for L<sup>A</sup>T<sub>E</sub>X via CTAN as `classicthesis`.”

<sup>3</sup> Emacs originally was an acronym for Editor MACroS. The first Emacs was a set of macros written in 1976 at MIT by Richard Stallman for the editor TECO (Text Editor and COrrector). The current version of Emacs, GNU Emacs, was originally written in 1984. GNU Emacs is an highly extensible and customizable text editor. Visit [www.gnu.org/software/emacs/](http://www.gnu.org/software/emacs/).